

1 **Reply to comments from Dr. Schaepli**

2 **General comment**

3 **1. This paper is a re-submission of a paper previously discussed in HESSD. The authors**  
4 **made a considerable effort to revise the text and the model to meet the reviewers'**  
5 **concerns. The model now has a separated degree-day factor for snow and ice and the**  
6 **description of the model is clearer (but still not entirely clear).**

7 *Reply: Thanks.*

8 **2. The proposed step-wise calibration method is tested to show how robust it is if applied**  
9 **to different periods and with different hydrograph separation criteria. The method**  
10 **is certainly transferable to other catchments and interesting for the readership of**  
11 **HESS and I recommend publication in HESS after minor revisions.**

12 *Reply: Thanks.*

13 **3. Before giving some detailed comments hereafter, I would like to point out here that**  
14 **I do not agree with the authors' view that an observed time series can be manipulated**  
15 **such as to "expand the measurement dimension". Information can be extracted from**  
16 **data but the information content of data cannot be increased by any manipulation.**  
17 **Could you please comment on this?**

18 *Reply: Thank you for this suggestion. We have modified the related concepts in the paper.*  
19 *'measurement dimension' has been modified as 'signature dimension' in the revised paper.*

20 **Detailed comments:**

21 **1. Abstract**

22 **1.1. In the abstract, the hydrograph is partitioned according to water sources but then**  
23 **"the hydrological model parameters are grouped by the associated \*runoff**  
24 **generation mechanism\*"; please use coherent wording according to the very first**  
25 **review of the 1<sup>st</sup> submission to HESSD. Same holds for section 3, and for the**  
26 **conclusion.**

27 *Reply: We have modified the 'runoff generation mechanism' as 'runoff water sources' in*  
28 *the revised paper.*

29 **1.2. The abstract does not mention any results, conclusions or outlooks, simply**  
30 **summarizes the method.**

31 *Reply: We have expanded the abstract section by adding more details about the results*

32 *and conclusions:*

33 *“Results show that the proposed calibration approach performed reasonably well. Cross*  
34 *validation and comparison to an automatic calibration method indicated its robustness.”*

35 **2. Introduction:**

36 **2.1. Good literature summary.**

37 *Reply: Thanks.*

38 **2.2. I do not agree with wording “hydrograph partitioning is another possible way to**  
39 **expand RM”. The measurement dimension cannot be expanded otherwise than by**  
40 **adding data; hydrograph partitioning might help to extract the meaningful**  
41 **information pieces and to match them with the corresponding parameter groups.**  
42 **This helps in parameter search since the parameters are not trying to match a piece**  
43 **of information which they are not supposed to simulated. But this does not “add**  
44 **measurements” and the measurement dimension is thus not expanded.**

45 *Reply: We have done the related modification in the revised paper by replacing the*  
46 *‘measurement dimension’ with the ‘signature dimension’. Here this sentence has been*  
47 *corrected as “However, glacier mass data and baseflow data are usually not available in*  
48 *some mountain basins. In these cases, hydrograph partitioning is another possible way to*  
49 *exploit information from available data.” in the revised paper.*

50 **3. Case study**

51 **3.1. I re-iterate my comment: why is the case study qualified as “alpine”? For botany,**  
52 **“alpine” might be a general term referring to any high elevation mountain range, for**  
53 **hydrology, “alpine” refers to my understanding to a hydro-climatic regime with a**  
54 **winter season with snow accumulation and a summer season with melt occurring due**  
55 **to high temperatures; is this the case here? Or do we have a regime where**  
56 **accumulation and melt occur both during the summer as in the Himalaya? On web**  
57 **of science, I could find a single paper mentioning the words “alpine hydrology and**  
58 **Tianshan”. Could you not just say why the area has alpine hydrology? Or simply**  
59 **replace alpine area by mountainous area? Namely also on p. 13398 and 13399 where**  
60 **the more general “mountainous area” should be used instead of alpine.**

61 *Reply: To the authors’ understanding, the term ‘alpine’ is an alternative word (and short)*

62 *for high mountain area. It has no hydrological meaning in this manuscript as referred by*  
63 *the Referee. Thanks for your suggestion. To avoid misunderstanding, we have replaced all*  
64 *the word “alpine” with the word “mountain” or “mountainous” in the revised paper.*

#### 65 **4. Method**

66 **4.1. I still do not understand how you connect the accumulation and melt of snow with**  
67 **the modis image. The paper says that snow accumulation and potential melt are**  
68 **simulated per subcatchment, I conclude that SWE is also computed per**  
69 **subcatchment. How do you connect this to the area that experiences melt as obtained**  
70 **from the MODIS image? Do you multiply the potential melt (mm/day) with the area**  
71 **that experiences melt? But then, how do you update the SWE? What do you do if**  
72 **your computed SWE is non-zero but the MODIS image does not show any snow**  
73 **pixels? And what if SWE is zero but MODIS shows snow?**

74 *Reply: In response to this comment, we have added the below discussion in the revised*  
75 *paper:*

76 *“To be noted, snowfall in each subcatchment is calculated according to the daily*  
77 *precipitation and temperature. And snowmelt is simulated using the degree-day method.*  
78 *However, the snow water equivalent in the snow cover zone (non-glacier area) is not*  
79 *computed. The existing of snow cover in each subcatchment is only determined by MODIS*  
80 *snow image. When the MODIS image indicates the existing of snow cover and meanwhile*  
81 *the daily temperature is higher than 0 °C, then snowmelt will occur, otherwise, snowmelt*  
82 *will not occur. The identification of snow cover by MODIS image is in accordance with*  
83 *the fact that the partitioning of snowmelt dominant hydrograph is based on MODIS snow*  
84 *products. If the existing of snow cover is determined by snow water equivalent, the*  
85 *temperature parameters to calculate snowfall can have significant effects on the estimation*  
86 *of the degree-day factor for snowmelt. To partly reduce this effect, we calibrate the degree-*  
87 *day factor for snowmelt on the basis of MODIS snow cover products. Although in this way,*  
88 *the water balance of snow cover is not taken into account in the snow cover zone, it should*  
89 *not impact the calibration of the degree-day factor for snowmelt. It’s worth noting that*  
90 *snow water balance in the glacier zone is updated by calculation of snow water equivalent*  
91 *where snow cover level should be relatively low.”*

92 **4.2. The use multi-letter parameter names is banned by HESS.**

93 *Reply: Thanks, we have modified all the multi-letter parameter names into subscripts.*

94 *'KKA' is corrected to 'K<sub>A</sub>', 'KKD' is corrected to 'K<sub>D</sub>' and 'WM' is corrected to 'W<sub>M</sub>'.*

95 **5. Results**

96 **5.1. I recommend explicitly commenting on the fact that clearly, the automatic calibration**  
97 **cannot find the solution to the optimization problem, otherwise it \*HAS\* to find a**  
98 **solution that is better than the step-wise solution. If the automatic solution found by**  
99 **optimizing NSE has a lower NSE or higher RMSE than the manual calibration, this**  
100 **means that the algorithm could not find the optimum.**

101 *Reply: In response to this comment, we have added the discussion below in the revised*  
102 *paper:*

103 *"The automatic calibration algorithm has run for about 5 weeks (840 hour on a desktop*  
104 *equipped with an Intel Core i7 CPU with 2.8GHz) to obtain the current results. Its*  
105 *performance can increase if the algorithm keeps on running, and even get higher*  
106 *performance than the step-wise calibration method. The comparison here is intending to*  
107 *show that the step-wise calibration method based on hydrograph partition can achieve*  
108 *considerable performance more effectively. The automatic algorithm here treats all the*  
109 *parameters equally during the calibration period. Each parameter should be optimized*  
110 *when searching for the optimal parameter set. This searching algorithm hampers the*  
111 *efficiency of the calibration procedure without identifying the dominant sub-periods for*  
112 *different parameters. In the step-wise calibration method, only parameters that are*  
113 *responsible for the simulation of corresponding hydrograph partition are optimized in*  
114 *each step. And also the calibration of parameter by this method reflects the role of each*  
115 *parameter for the basin runoff generation."*

116 **5.2. Again, I do not agree with the wording "Benefitting from the partitioning curves,**  
117 **however, the stepwise calibration method increases the dimension of measurement**  
118 **information to four. The measurement dimension is now equal to the number of**  
119 **parameter groups," The information content of data cannot be expanded by data**  
120 **manipulation. It can only be extracted. Otherwise you would create information.**

121 *Reply: In the revised paper, we have revised this sentence as "Benefitting from the*

122 *partitioning curves, however, the stepwise calibration method increases the dimension of*  
123 *hydrological signature to four. The signature dimension is now equal to the number of*  
124 *parameter group.”*

125 **5.3. What means “to extracting index information”?**

126 *Reply: it have been corrected as “to extract hydrological signatures”.*

127

128 **Reply to comments from Dr. Zappa**

129 **Remarks:**

130 **1. This manuscript is a re-submission of I manuscript I already evaluated in March 2014.**

131 **The original manuscript was already rather interesting concerning topic and concepts,**  
132 **but rather unripe in its realization, analysis and presentation. In this new version the**  
133 **problematic issues have been addressed.**

134 *Reply: Thanks.*

135 **2. In its current form the paper is very well embedded in scientific literature on the topic.**

136 **Also the description of the test area is well documented and referenced. As in the**  
137 **original manuscript I appreciate the use of field data for estimating the lapse rates**  
138 **(Sections 2.2.1 and 2.2.2). This is a nice example of confining uncertainty by adding**  
139 **additional information from observations.**

140 *Reply: Thanks.*

141 **3. Concerning the improvements we have now in Table 5 a good overview including**  
142 **calibration and evaluation periods.**

143 *Reply: Thanks.*

144 **4. In the original submission I was complaining because I found your model was not able**  
145 **to capture peaks due to storm rainfall and rapid reaction by the basin. In this version**  
146 **I found this issue is almost solved. Did you some adjustments in the process**  
147 **description? Or is this an improvement stemming from the changes in the snowmelt**  
148 **and icemelt components (Page 13402)?**

149 *Reply: The model has been slight modified in Section 3.2. We have improved the process*  
150 *for runoff generated from rainfall directly in glacier area in the model. Given the relative*  
151 *large glacier coverage and the steep terrain in the study basin, rainfall provides storm*  
152 *runoff and flows into the stream network directly, which flows into the bare soil zone and*  
153 *reaches the stream network slowly in the previous model. The simulation of peak flows have*  
154 *been improved significantly benefiting from these modifications.*

155 **Points to be addressed:**

156 **1. I already mentioned in the original submission, that you should be careful in defining**  
157 **your partition a “dominant runoff mechanism”. In this manuscript you confuse and**

158 **mix this again. I remember we suggested to use “dominant source of water”.**

159 *Reply: Thanks. We have modified all the ‘runoff generation mechanism’ as ‘runoff water*  
160 *sources’ in the revised paper.*

161 **2. On page 13400 you present your rules to separate the hydrograph. In Figure 6 we see**  
162 **the temporal distribution of the 4 options presented in Eq. 6. I understand you want**  
163 **to keep the rules easy, but if I correctly interpret Figure 6 you have surely small rain**  
164 **events in April. The red and green categories are very marginal in your test area, as**  
165 **they should focus on temperature driven snow and icemelt short before and short**  
166 **after the rain season. How do these rain events with obvious generation of  $Q_r$  affect**  
167 **your calibrated data sets?**

168 *Reply: Given the seasonality of precipitation in our test area (shown in Figure 3), we*  
169 *neglected the rain events in the period from October to April for the test of the proposed*  
170 *calibration method. We acknowledge that this is a rough assumption, and surely small rain*  
171 *events will occur during this period. To take the effects of these rain events on the*  
172 *calibration into account, an iteration calibration procedure is adopted in this study. The*  
173 *parameters for melt and rainfall runoff are firstly calibrated on their dominant hydrograph*  
174 *parts (red and green, blue in Figure 6) separately, then the melt parameters are re-*  
175 *calibrated on the basis of the calculation of rainfall runoff using the parameters already*  
176 *calibrated in the first step. This calibration procedure is repeated until the parameter*  
177 *values getting a stable level. In this way, the effects of rainfall events in April on the*  
178 *calibration can be partly taken into account. And also, we have done some work to evaluate*  
179 *the sensitivity of the calibration to the partition of the rainfall event dominant hydrograph*  
180 *in Section 4.5. Results in Table 6 and Figure 10 show the rainfall events can have an*  
181 *important role on the calibration on the rainfall runoff parameter (i.e. WM), while have*  
182 *relatively slighter effects on the calibration of melt and groundwater parameters. The*  
183 *accurate partition of the rainfall runoff dominant hydrograph should be improved based*  
184 *on the more accurate measurement of rainfall in the test area, which can be working for*  
185 *further study.*

186 **3. 13403: As table 6 demonstrate their sensitivity to your approach, can you give some**  
187 **more information on the meaning of KKA and KKD. You call both of them**

188 “coefficient used to calculate calibrated subsurface flow”, which is for me no useful  
189 information. Are the two factors linkable to some physical property (infiltration,  
190 storage coefficient or so?)

191 *Reply: We have added the below sentence in Section 3.2 in the revised manuscript:*

192 “ $K_A$  and  $K_D$  are outflow coefficients of groundwater storage. Their sum determines the flow  
193 rate of groundwater baseflow and their ratio ( $K_D / K_A$ ) dominate the proportion of free  
194 groundwater storage. Infiltration and storage should have effects on the calibration of the  
195 two parameters. ”

196 **Minor issues:**

197 **1. 13390-15: Typo: “slope”**

198 *Reply: We have revised it.*

199 **2. 13400: The notation chosen in Equation 6 is rather odd (minus signs in the indices to**  
200 **describe the mathematical equivalence). It is surely how you implemented it in your**  
201 **algorithm, but it is not very elegant in a manuscript. Wouldn’t be better to have**  
202 **maybe a table instead?**

203 *Reply: We have improved it in the form as follow in the revised manuscript:*

$$204 \quad Q = \begin{cases} Q_{SB} & \text{for } S_i=0, G_i=0, \text{ and } D_i = 0 \\ Q_{SB} + Q_{SM} & \text{for } S_i=1, G_i=0, \text{ and } D_i = 0 \\ Q_{SB} + Q_{SM} + Q_{GM} & \text{for } S_i=1, G_i=1, \text{ and } D_i = 0 \\ Q_{SB} + Q_{SM} + Q_{GM} + Q_R & \text{for } D_i = 1 \end{cases}$$

205 **3. Table 3: on which basis you decide to have identical hydraulic conductivity in the u-**  
206 **zone and s-zone?**

207 *Reply: The soil layer in the test area is very thin. Soil storage capacity is relative low.*  
208 *Subsurface flow is mainly generated from groundwater. To make the simulation of*  
209 *subsurface flow simple, we assumed the hydraulic conductivity of the u-zone is same to the*  
210 *s-zone.*

211 **Final considerations:**

212 **I thank the authors for having made the effort to invest some more time to improve this**  
213 **manuscript. I listen now only few point they should now address. If this is achieved then**  
214 **I can recommend the paper for acceptance.**



215 *Reply: Thanks. The related points have been addressed in the revised manuscript.*  
216

217 **List of relevant changes.**

218 Dear Editor,

219 This is a revised version of the hessd-11-13385-2014 paper. In making the new version of the  
220 paper, we have carefully addressed all the comments and suggestions provided by two Referees  
221 (i.e. Dr. Schaefli and Dr. Zappa). In response to the concern on the using of MODIS snow cover  
222 image in the model by Dr. Schaefli, we have added some new sentences in Section 3.2 to  
223 describe the connecting between accumulation and melt of snow and MODIS image in more  
224 detail. We have also corrected all of the “runoff generation mechanism” as “runoff water  
225 sources” in the revised manuscript, as pointed out by both the two Referees. In response to other  
226 minor comments by the two Referees, we have also added some sentences and corrected some  
227 words in this new manuscript. In particular:

- 228 1) We have added some details about the study results in the abstract section.
- 229 2) The related “measurement dimension” have been modified as “signature dimension”  
230 in the revised manuscript.
- 231 3) The word “alpine” has been replaced with “mountain” or “mountainous”.
- 232 4) We have modified the multi-letter parameter names into subscripts. i.e., ‘ $KKA$ ’ is  
233 corrected to ‘ $K_A$ ’, ‘ $KKD$ ’ is corrected to ‘ $K_D$ ’ and ‘ $WM$ ’ is corrected to ‘ $W_M$ ’.
- 234 5) In response to the comments on the automatic calibration algorithm by Dr. Schaefli,  
235 we have added a discussion paragraph in Section 4.3.
- 236 6) We have added some sentences to describe the meaning of parameter  $K_A$  and  $K_D$  in  
237 Section 3.2 in response to the comments by Dr. Zappa.
- 238 7) The format of Equation 6 have been improved, as pointed out by Dr. Zappa.

239 Thank you very much for your attention and consideration. The revised new manuscript is  
240 presented as follows, and all the changes have been marked as red.

241 Sincerely yours,

242 Fuqiang TIAN

243 Department of Hydraulic Engineering, Tsinghua University, Beijing 100084

244 **Diagnostic calibration of a hydrological model in a mountain**  
245 **area by hydrograph partitioning**

246 Z. H. He<sup>1</sup>, F. Q. Tian<sup>1\*</sup>, H. V. Gupta<sup>2</sup>, H. C. Hu<sup>1</sup>, H. P.Hu<sup>1</sup>

247

248

249 1. State Key Laboratory of Hydrosience and Engineering, Department of Hydraulic  
250 Engineering, Tsinghua University, Beijing 100084, China

251 2. Department of Hydrology and Water Resources, The University of Arizona,  
252 Tucson, Arizona, 85721, USA

253

254 \*Corresponding author information:

255 Email: [tianfq@tsinghua.edu.cn](mailto:tianfq@tsinghua.edu.cn)

256 Tele: +86 010 6277 3396

257 Fax: +86 010 6279 6971

258

259

260

261 Manuscript submitted to Hydrology and Earth System Sciences

262 2015.03.02

263 **Abstract**

264 Hydrological modeling can exploit informative signatures extracted from long time sequences  
265 of observed streamflow for parameter calibration and model diagnosis. In this study we explore  
266 the diagnostic potential of hydrograph partitioning for model calibration in mountain areas,  
267 where meltwater from snow and glaciers are important sources for river runoff (in addition to  
268 rainwater). We propose an index-based method to partition the hydrograph according to  
269 dominant runoff water sources, and a diagnostic approach to calibrate a mountain hydrological  
270 model. First, by accounting for the seasonal variability of precipitation and the altitudinal  
271 variability of temperature and snow/glacier coverage, we develop a set of indices to indicate  
272 the daily status of runoff generation from each type of water source (i.e., glacier meltwater,  
273 snow meltwater, rainwater, and groundwater). Second, these indices are used to partition a  
274 hydrograph into four parts associated with four different combinations of dominant water  
275 sources (i.e., groundwater, groundwater + snow meltwater, groundwater + snow meltwater+  
276 glacier meltwater, groundwater + snow meltwater + glacier meltwater + rainwater). Third, the  
277 hydrological model parameters are grouped by the associated runoff sources, and each group is  
278 calibrated to match the corresponding hydrograph partition in a stepwise and iterative manner.  
279 Similar to use of the regime curve to diagnose seasonality of streamflow, the hydrograph  
280 partitioning curve based on a dominant runoff water source (more briefly called the partitioning  
281 curve, not necessarily continuous) can serve as a diagnostic signature that helps relate model  
282 performance to model components. The proposed methods are demonstrated via application of  
283 a semi-distributed hydrological model (THREW) to the Tailan River basin (1324 km<sup>2</sup>) in the  
284 Tianshan Mountain of China. **Results show that the proposed calibration approach performed**  
285 **reasonably well. Cross validation and comparison to an automatic calibration method indicated**  
286 **its robustness.**

## 287 **1 Introduction**

### 288 **1.1 Background**

289         Parameter calibration has been singled out as one of the major issues in the application of  
290 hydrological models (Johnston and Pilgrim, 1976; Gupta and Sorooshian, 1983; Beven and  
291 Binley, 1992; Boyle *et al.*, 2000). Commonly, one or more objective functions are selected as  
292 criteria to evaluate the similarity between observed and simulated hydrographs (Nash and  
293 Sutcliffe, 1970; Brazil, 1989; Gupta *et al.*, 1998; van Griensven and Bauwens, 2003). As model  
294 complexity increases, parameter dimensionality also increases significantly, which makes it  
295 much more difficult to calibrate model parameters manually. For this reason, automatic  
296 calibration procedures have been developed to identify the optimal parameter set (Gupta and  
297 Sorooshian, 1985; Gan and Biftu, 1996; Vrugt *et al.*, 2003a,b). However, due to limitations in  
298 process understanding and measurement technologies, one can find different parameter sets  
299 within a chosen space that may acceptably reproduce the observed aspects of the catchment  
300 system (Sorooshian and Gupta, 1983; Beven and Freer, 2001). This phenomenon, which has  
301 been called “equifinality”, causes uncertainty in simulation and prediction (Duan *et al.*, 1992;  
302 Beven, 1993, 1996), and highlights the need for methods that are powerful enough to  
303 ‘diagnostically’ evaluate and correct models, i.e., that are capable of indicating to what degree  
304 a realistic representation of the real world has been achieved and pointing towards how the  
305 model should be improved (Spear and Hornberger, 1980; Gupta *et al.*, 1998, 2008).

306         Traditional regression-based model evaluation strategies (e.g., based on the use of Mean  
307 Squared Error or Nash Sutcliffe Efficiency as performance criteria) are demonstrably poor in  
308 their ability to identify the roles of various model components or parameters in the model output  
309 (Van Straten and Keesman, 1991; Zhang *et al.*, 2008; Gupta *et al.*, 2008; Yilmaz *et al.*, 2008;  
310 Hingray *et al.*, 2010), which is due in part to the loss of meaningful information when projecting  
311 from the high dimension of the data set (like hydrograph) down to the low (often one)  
312 dimension of the measure (Yilmaz *et al.*, 2008; Gupta *et al.*, 2009). A diagnostic evaluation  
313 method should match the number of unknowns (parameters) with the number of pieces of  
314 information by making use of multiple measures of model performance (Gupta *et al.*, 1998,  
315 2008, 2009; Yilmaz *et al.*, 2008). One way to exploit hydrological information is to analyze the  
316 spatiotemporal characteristics of hydrological variables that can be related to specific

317 hydrological processes in the form of “signature indices” (Richter *et al.*, 1996; Sivapalan *et al.*,  
318 2003; Gupta *et al.* 2008, Yilmaz *et al.*, 2008). Ideally, a “signature” should represent some  
319 “invariant” property of the system, be readily identifiable from available data, directly reflect  
320 some system function, and be maximally related to some “structure” or “parameter” in the  
321 model.

322 Attention to hydrological signatures, therefore, constitutes the natural basis for model  
323 diagnosis (Gupta *et al.*, 2008). Placed in this context, the body of literature on the topic is indeed  
324 large. Jothityangkoon *et al.* (2001) proposed a downward approach to evaluate the model’s  
325 performance against appropriate signatures at progressively refined time scale. Signatures that  
326 govern the evaluation of model complexity are the inter-annual variability, mean monthly  
327 variation in runoff (called regime curve), and the flow duration curve (FDC). Farmer *et al.*  
328 (2003) evaluated the climate, soil and vegetation controls on the variability of water balance  
329 through four signatures: gradient of the annual yield frequency graph, average yield over many  
330 years for each month, FDC, and magnitude and shape of the hydrograph. Shamir *et al.* (2005a)  
331 described a parameter estimation method based on hydrograph descriptors (total flow, range  
332 between the extreme values, monthly rising limb density of the hydrograph, monthly maximum  
333 flow and negative/positive change) that characterize dominant streamflow patterns at three  
334 timescales (monthly, yearly, and record extent). Detenbeck *et al.* (2005) calculated several  
335 hydrologic indices including daily flow indices (mean, median, coefficient of variation, and  
336 skewness), overall flood indices (flood frequency, magnitude, duration, and flood timing of  
337 various levels), low flow variables (mean annual daily minimum), and ranges of flow  
338 percentiles to study the relationship of the streamflow regime to watershed characteristics.  
339 Shamir *et al.* (2005b) presented two streamflow indices to describe the shape of the hydrograph  
340 (rising/declining limb density, i.e., RLD and DLD) for parameter estimation in 19 basins of  
341 United States. Yadav *et al.* (2007) used similarity indices and hydrological signatures (runoff  
342 ratio and slope of the FDC) to classify catchments. Westerberg *et al.* (2011) selected several  
343 evaluation points on the FDC to calibrate models, and compared two selection methods to  
344 evaluate their effects on parameter calibration.

345 Generally, the reported signatures have the following two characteristics: (1) they  
346 concentrate on the extraction of hydrologically meaningful information contained in

347 hydrographs, and (2) they focus on either an entire study period or a special continuous section  
348 of the entire period. They have occasionally considered temporal variability of runoff  
349 components and dominance of different runoff sources during different periods (e.g., the  
350 seasonal switching of runoff sources discussed in Tian *et al.*, 2012). However, a hydrograph  
351 could be dominated by various components or water sources at different response times  
352 (Haberlandt *et al.*, 2001; Eder *et al.*, 2005). Within this in mind, a few studies have explored  
353 the use of hydrological information in time dimension for stepwise calibration. For example,  
354 Schaefli *et al.* (2005) presented a stepwise calibration method for 7 parameters in a high  
355 mountainous area: snow and ice melt degree-day factors were conditioned by mass balance,  
356 slow reservoir parameters were determined by base flow, reservoir coefficients were calibrated  
357 by summer runoff, and the direct runoff coefficient was used to control discharge during  
358 precipitation events. Another notable example is Hingray *et al.* (2010), in which the authors  
359 estimated the value of snowmelt degree-day factor in a mountain basin by progressively  
360 minimizing the differences between observed and simulated values of different magnitude  
361 hydrographs. There are also many other follow up studies.

362 In mountain areas, streamflow is composed of both snow/glacier meltwater and rainwater.  
363 The energy-based and temperature-index models are two principal approaches to simulate snow  
364 and glacier melt (Rango and Martinec, 1979; Howard, 1996; Kane *et al.*, 1997; Singh *et al.*,  
365 2000; Fierz *et al.*, 2003). To describe significant heterogeneity of temperature, precipitation,  
366 snow, and glacier, distributed hydrological models are generally used for precipitation-runoff  
367 modeling in mountain regions (Daly *et al.*, 2000; Klok *et al.*, 2001 etc.). Also, the utilization of  
368 remotely sensing products of precipitation and snow cover data in the mountain runoff  
369 modeling has become more popular in recent years (Swamy and Brivio, 1997; Akyurek *et al.*,  
370 2011; Liu *et al.*, 2012 etc.). Most of these studies report sound simulation results. However, the  
371 need to develop an appropriate calibration strategy for precipitation-runoff modeling in  
372 mountain areas remains a key issue for two reasons: first, the hydrological processes are usually  
373 more complex (with snow/glacier melt and possibly soil freezing/thawing) than those in warmer  
374 areas, which implies a larger dimension of parameter ( $R^P$ ) in the corresponding hydrological  
375 model; second, measured data set useful for model identification is usually limited due to a  
376 sparse gauge network, which produces a small measurement dimension ( $R^M$ ) far lower than  $R^P$ .

377 To address this problem, related studies are putting effort into two directions. One is to reduce  
378 the calibrated  $R^P$  by estimating some of the parameters based on basin characteristics *a priori*.  
379 For example, Gurtz *et al.* (1999) proposed a parameterization method based on elevation, slope  
380 and shading derived from basin terrain. Gomez-Landes and Rango (2002) obtained model  
381 parameters of ungauged basins from gauged basins by basin size, proximity of location, and  
382 shape similarities. Eder *et al.* (2005) estimated most of the parameters *a priori* from basin  
383 physiography before an automatic calibration was applied. The parameterization method may  
384 involve some uncertainties but be useful for the determination of insensitive parameters.

385 The second direction is to exploit hydrological information from implicit measure data.  
386 For instance, Dunn and Colohan (1999) used baseflow data as additional criteria for model  
387 evaluation. Mendoza *et al.* (2003) exploited recession-flow data to estimate hydraulic  
388 parameters. Stahl *et al.* (2008) used glacier mass balance information combined with stream  
389 hydrographs to constrain melt factors. Huss *et al.* (2008) used annual ice volume change data  
390 for optimizing melt and radiation factors, and glacier equilibrium line altitude for precipitation  
391 correction factors. Schaepli and Huss (2011) integrated the seasonal information of point glacier  
392 mass balance for model calibration by modifying the GSM-SOCONT model. Jost *et al.* (2012)  
393 introduced glacier volume loss calculated by high-resolution digital elevation models to  
394 calibrate hydrologic model. Knowledge acquired from the aforementioned research indicates  
395 that the use of additional information (e.g., baseflow, recession flow, and glacier mass balance)  
396 can effectively help reduce parameter uncertainty by significantly expanding  $R^M$ .

397 However, glacier mass data and baseflow data are usually not available in some mountain  
398 basins. In these cases, hydrograph partitioning is another possible way to exploit information  
399 from available data. Information about dominant hydrological processes contained in a  
400 hydrograph can be extracted by hydrograph partitioning or separation; this has long been a topic  
401 of interest in hydrology. Several different kinds of methods have been proposed (Pinder and  
402 Jones, 1969; McCuen, 1989; Nathan, 1990; Arnold *et al.*, 1995, 1999; Vivoni *et al.*, 2007),  
403 which can generally be classified into graphical methods, analytical methods, empirical  
404 methods, geochemical methods and automated program techniques (Nejadhashemi *et al.*, 2009).  
405 Most of them primarily focus on the partitioning of baseflow and are not capable of identifying  
406 more than two components. With the advent of isotope methods, multi-component hydrograph



407 separation models have been developed. However, these models need be run for an extended  
408 period of time (usually a minimum of one hydrologic year) for the assumption that the isotopes  
409 of components are conserved to hold (Hooper and Shoemaker, 1986) and call for volumes of  
410 field data that are seldom available in poorly gauged and difficult to access mountain basins.

## 411 **1.2 Objectives and Scope**

412 This paper explores the benefits of partitioning the hydrograph into several parts, each  
413 related to one combination of dominant water sources for runoff generation. The parameter  
414 group controlling each type of runoff sources is then calibrated using the corresponding  
415 partitioning hydrographic curves via a stepwise approach, and model deficiencies are diagnosed  
416 by evaluating the model simulations associated with each partitioning curve (as a diagnostic  
417 signature). We demonstrate the potential of this approach in a mountain area where streamflow  
418 is the result of complex runoff generation processes arising from combinations of storm events  
419 and snow/glacier melt. The influence of each type of water source (groundwater, snow  
420 meltwater, glacier meltwater, or rainwater) varies in time and can be determined by an analysis  
421 of the dynamic spatiotemporal information in the available data series.

422 The paper is organized as follows. Section 2 contains a description of the geographic and  
423 hydrological characteristics of the study basin, including the main data sources and data  
424 preprocessing. Section 3 details the proposed method of hydrograph partitioning and parameter  
425 calibration based on a semi-distributed model coupled with the temperature-index method.  
426 Section 4 presents the results and discusses the possible sources of uncertainty. Section 5  
427 provides a summary of this study and discusses further applications of the partitioning strategy.

## 428 **2 Study Area and Data**

### 429 **2.1 Overview of the Study Area**

430 The study mountain area (Tailan River basin, TRB) is on the south slope of the Tianshan  
431 Mountain (one of the highest mountain areas in China) in the Xinjiang Uygur Autonomous  
432 Region of China and extends from 41° 35'N to 42° 05' N and 80° 04'E to 80° 35'E, covering a  
433 drainage area of 1324 km<sup>2</sup>. Elevation ranges from 1600 m to 7100 m a.s.l. with an average  
434 value as high as 4100 m a.s.l. Precipitation occurs mainly in summer and rarely in winter, and  
435 winter precipitation always comes in the form of snowfall. Snow coverage accumulates in  
436 winter and ablates from spring into late summer when it melts away completely; the snow

437 coverage dynamics can be obtained from MODIS data (see Figure 4). The basin is highly  
438 glacierized with approximately 33% of the basin area covered by glacier ice (see Figure 1). The  
439 glacier coverage stretches from approximately 3000 m to 7100 m a.s.l. and exists mainly at an  
440 altitude range of 4000 m to 5000 m a.s.l. Glacier melt and snowmelt form runoff as long as the  
441 temperature rises above a certain threshold and provide primary sources for downstream  
442 discharge.

443 TRB is a heavily studied mountain watershed in northwestern China. The relevant  
444 literature (Kang and Zhu, 1980; Shen *et al.*, 2003; Xie *et al.*, 2004; Gao *et al.*, 2011; Sun *et al.*,  
445 2012) are reviewed below, and the main conclusions about the hydrometeorological  
446 characteristics are summarized as follows:

447 (1) The climate presents strong altitudinal variability. The mean annual precipitation in  
448 higher mountain areas is approximately 1200 mm (Kang *et al.*, 1980), while it is approximately  
449 only 180 mm in the outlet plain area (Xie *et al.*, 2004). The mean annual temperature ranges  
450 from below 0°C in mountain areas to approximately 9°C at the basin outlet (Sun *et al.*, 2012).

451 (2) Meltwater is the principal source of streamflow. Snow and glacier meltwater account  
452 for approximately 63% of the annual runoff (Kang *et al.*, 1980). The contribution of rainwater  
453 is relatively lower and occurs mainly in the storm rain period (May to September) (Xie *et al.*,  
454 2004). Groundwater baseflow is smaller but dominates the streamflow in the winter (January,  
455 February and December), during which either rainfall or melt rarely occur (Kang *et al.*, 1980).

456 (3) The TRB river network is a simple fan system. Given large topographic drop and  
457 moderate drainage area, the runoff concentration time is no longer than one day (Xie *et al.*,  
458 2004). Melting and falling water can quickly flow into the main channel and reach the basin  
459 outlet.

## 460 **2.2 Data & Preprocessing**

461 The Tailan gauging station (THS, 1602 m a.s.l.) is located the outlet of the watershed,  
462 where runoff, precipitation and temperature have been measured since 1957. To collect  
463 temperature and precipitation data at higher elevation, two automatic weather stations (AWS,  
464 product type TRM-ZS2) were set up in June 2011 (i.e., XT AWS, at 2116 m a.s.l. and TG AWS,  
465 at 2381 m a.s.l.). This relatively short record (from July 1, 2011-December 31, 2012) was used  
466 to estimate the lapse rate of precipitation and temperature (see below). The Bingtan automatic

467 weather station (BT AWS, at 3950 m a.s.l.) located in an adjacent catchment (Kumalak basin)  
 468 was used to validate the estimated temperature lapse rates. A digital elevation model (DEM)  
 469 with a spatial resolution of 30 m was provided by the International Scientific & Technical Data  
 470 Mirror Site, Computer Network Information Center of the Chinese Academy of Sciences  
 471 (<http://www.gscloud.cn>). Remotely sensed snow cover area (SCA) data were downloaded from  
 472 the MODIS website; the MOD10A2 and MYD10A2 products were used, both of which have a  
 473 spatial resolution of 500m and a temporal resolution of eight-days. Daily snow cover data was  
 474 obtained by linear interpolation of the eight-day data. The China Glacier Inventory (CGI) (Shi,  
 475 2008) was used to derive glacier coverage in the TRB. In our experience, most of the snow  
 476 melts away after the warm summer period and the lowest snow/ice coverage in the year should,  
 477 therefore, be roughly equal to the glacier coverage. Based on an analysis of filtered MODIS  
 478 SCA (see Sect. 2.2.3), the lowest values of snow/ice coverage in the study period (2003-2012)  
 479 are almost the same, which indicates that TRB glacier coverage is relatively stable during the  
 480 study period. The DEM, river system, gauging stations and glacier distribution are shown in  
 481 Fig.1.

### 482 2.2.1 Temperature Lapse Rate

483 Altitudinal distribution of temperature can be estimated through the lapse rate (Rango and  
 484 Martinec, 1979; Tabony, 1985). According to Aizen *et al.* (2000), rates of temperature decrease  
 485 with increasing elevation are quite different in various months, and ignoring this difference may  
 486 lead to significant errors in the simulation of snow accumulation and melt. The lapse rate was  
 487 therefore estimated for each month. Temperature variations with altitude can be estimated by  
 488 the following equation, i.e.:

$$489 \quad T = T_o + T_p \cdot (H - h) \quad (1)$$

490 where,  $T_o$  is the temperature value at low altitude (THS in this study), and  $T_p$  is the  
 491 temperature lapse rate (usually negative),  $H$  and  $h$  are the elevation values at high and low  
 492 positions, i.e., the mean elevation of two AWS and the elevation of THS, respectively. The  
 493 values of  $T_p$  in different months are obtained by minimizing the error function, i.e.:

$$494 \quad \min : z = \sum (T_i - (T_{oi} + T_p \cdot (H - h)))^2 \quad (2)$$

495 where,  $i$  indicates the  $i^{th}$  day in the analyzed month,  $T_i$  is the observed temperature in AWS,

496 which is the mean value of the TG AWS and XT AWS in this study.

497 The temperature series data from July 1, 2011 to December 31, 2012 at THS, TG AWS  
498 and XT AWS were used to estimate the temperature lapse rate. The results (Table1) indicate  
499 significant month-to-month variation ranging from  $-0.30^{\circ}\text{C } 100 \text{ m}^{-1}$  in December to  $-0.86^{\circ}\text{C } 100$   
500  $\text{m}^{-1}$  in August. To validate the temperature lapse rates, the estimated and observed temperature  
501 data at BT AWS were compared (Fig. 2). We also compared the estimated temperature by an  
502 annual constant lapse rate ( $-0.62^{\circ}\text{C } 100 \text{ m}^{-1}$ , a similar value to previous studies, e.g., Tabony  
503 (1985) and Tahir *et al.*(2011)). This constant value is optimized by the same method in Eqn. (2)  
504 but using all daily temperature measurements. Figure 2 indicates that the monthly lapse rate  
505 method performs better than the annual constant rate method at the BT station for all months  
506 throughout the year. Further, the temperature curves estimated by monthly lapse rates for April  
507 to August match the observed ones rather well. Note that the estimated temperatures tend to  
508 underestimate observed ones for the rest of the months, which, however, will not affect the melt  
509 runoff significantly due to the general freezing condition during this period.

### 510 **2.2.2 Precipitation Lapse Rate**

511 Based on the precipitation series measured at THS, the monthly precipitation to annual  
512 precipitation ratio (Fig.3) for the study period (2003-2012) indicates that precipitation occurs  
513 mainly in May to September. The lapse rate of precipitation was also estimated monthly, and a  
514 similar procedure as temperature was applied. The different is that the precipitation analysis  
515 was conducted at a weekly rather than daily time step, and the maximum measured precipitation  
516 of the two installed AWS was used instead of the mean value. The analyzed period is limited  
517 to the storm rain period (May to September). Other months are not included due to the relatively  
518 small precipitation amount. The weekly precipitation lapse rates are listed in Table2. Daily  
519 precipitation differences between higher and lower altitudes can be estimated as the weekly  
520 precipitation lapse multiplied by the ratio of daily precipitation to the corresponding weekly  
521 amount in THS. The precipitation lapse rate was not validated against BT AWS because of  
522 significant differences in precipitation distribution between the two basins (i.e., Tailan and  
523 Kumalak).

### 524 **2.2.3 Filtering of MODIS Snow Cover Area Data**

525 Snow cover extent was obtained from MODIS products. The MOD10A2 and MYD10A2

526 products were downloaded from the website <http://reverb.echo.nasa.gov>. In total, we obtained  
527 460 eight-day images (two tiles, h23v04 and h24v04) from 2003 to 2012 for each product.  
528 Given that the accuracy of the MODIS SCA product is affected by cloud coverage to a  
529 significant degree, the remotely sensed images should be filtered to avoid the noise from clouds  
530 before using it for hydrological modeling (Ackerman *et al.*, 1998). The following three  
531 successive steps are adopted to filter the products based on previous reports (Gafurov and  
532 Bardossy, 2009; Wang *et al.*, 2009; Lopez-Burgos *et al.*, 2012):

533 (1) Satellite combination: The snow cover products of two satellites, Terra (MOD10A2)  
534 and Aqua (MYD10A2) were combined. As long as the value of a pixel is marked as snow in  
535 either satellite, the pixel value is marked as snow.

536 (2) Spatial combination: Inspecting the values of the nearest four pixels around one center  
537 pixel marked as cloud, if at least three of the four surrounding pixels are marked as snow, the  
538 center pixel is modified as snow.

539 (3) Temporal combination: If one pixel is marked as cloud, its values in the previous and  
540 following observations are investigated. If both of the two observed values are snow, then the  
541 present value of the same pixel is snow.

542 As an example, the filtered results from year 2004-2005 shown in Fig.4 demonstrate a  
543 significant reduction in fluctuation of the SCA products. We find that the lowest values of  
544 snow/ice coverage in all years (2003-2012) are relatively stable (from 2003 to 2012 are: 35%,  
545 34%, 39%, 36%, 37%, 34%, 41%, 35%, 38%, 39%, showing no obvious trend), which is close  
546 to the glacier coverage area (33%) derived from the CGI data mentioned in Sect.2.2. As  
547 mentioned before, MODIS snow/ice covered area in later summer is mainly composed of  
548 glacier coverage when snow has been melt away completely. The filtered results indicate a  
549 relatively stable coverage of glacier in TRB.

#### 550 **2.2.4 Altitudinal Cumulative Melt Curve**

551 The daily temperature of each cell in MODIS SCA images can be estimated by a  
552 temperature lapse rate based on its elevation and daily temperature measured at THS. As long  
553 as the temperature exceeds a specific threshold value for melt (assumed to be 0°C in this study),  
554 a given cell was labeled as an active cell in terms of melt. The land cover type for each cell was  
555 classified into glacier, snow, and other land cover according to the CGI and MODIS SCA

556 product. To obtain the area covered by snow only, we subtracted the glacier area in CGI from  
557 the SCA (a similar procedure can be found in Luo *et al.*, 2013). When a glacier or snow cover  
558 cell is active, it is labeled as a melt cell, and the melt area is computed as the number of active  
559 cells multiplied by the area of a cell.

560 Organizing the melt area by elevation from low to high and summing the melt area at each  
561 elevation, we can get the altitudinal cumulative melt curve, which can be used to describe the  
562 spatiotemporal distribution of melt area. The altitudinal cumulative melt curves calculated from  
563 2003 to 2012 for all months (Fig.5) show that melt mainly occur from May to September, which  
564 coincides with the precipitation period. Snowmelt starts at an elevation of approximately 1650  
565 m a.s.l., while glacier melt starts at an elevation of approximately 2950 m a.s.l, which has an  
566 important implication for hydrograph partitioning.

### 567 **3 Methodology**

568 Theoretically, every drop of water in the streamflow comes ultimately from precipitation.  
569 Practically, we can consider water sources for runoff generation in mountain areas as mainly  
570 consisting of meltwater from snow and glacier, rainwater, and groundwater. Groundwater at the  
571 basin scale is recharged by direct infiltration and run-on infiltration of meltwater or rainwater,  
572 and it is mainly discharged as baseflow via a subsurface flow path (especially in mountain areas  
573 where the large elevation gradient favors baseflow discharge). For the purpose of hydrograph  
574 partitioning, we can consider recharge to be a separate water source for streamflow, independent  
575 of meltwater and rainwater, which principally forms the baseflow part of a hydrograph. The  
576 remaining part of a hydrograph is principally formed by meltwater and rainwater via surface  
577 flow path (Blöschl *et al.*, 2013). We develop three indices to indicate the water sources for  
578 runoff generation at the daily time scale. The hydrograph is further partitioned into several sub-  
579 parts based on the indices values. Each sub-part is dominated by one or more water sources for  
580 runoff generation. With the partitioning hydrographic curves, the parameters of hydrological  
581 models are correspondingly grouped by runoff sources and calibrated in a stepwise fashion. We  
582 use the THREW model coupled with a temperature-index module as an exploratory tool. To  
583 better demonstrate usefulness of the proposed methods, only the runoff generation related  
584 parameters, which are also significantly sensitive parameters (see Sect.4.6), are calibrated.  
585 Other insensitive parameters are fixed at their initial values, specified *a priori* from the literature

586 or by expert knowledge.

### 587 **3.1 An Index-based Method for Hydrograph Partitioning**

588 In mountain areas, the relative contribution of different runoff water sources to the total  
589 streamflow varies throughout the year (Martinec *et al.*, 1982; Dunn and Colohan, 1999; Yang  
590 *et al.*, 2007). For the rainwater source, Fig.3 shows that precipitation in TRB presents strong  
591 seasonality and primarily concentrates (more than 76%) in the storm rain period from May to  
592 September. During the relatively dry period from October to April, mean precipitation gauged  
593 at the THS is just 43 mm, while precipitation in the higher mountainous region is mainly  
594 snowfall. Therefore, surface runoff induced by rainwater can rarely occur during relative dry  
595 period. It is reasonable to assume that the rainwater source can only contribute to the surface  
596 runoff part of a hydrograph on the same day during the storm rain period (May to September)  
597 except for the baseflow occurring much later.

598 For the meltwater sources, the altitudinal cumulative melt curves (Fig.5) show that the  
599 areas experiencing glacier melt and snowmelt change significantly with elevation. Melt of  
600 glacier and snow begins at different elevations in different months, i.e., glacier melt can only  
601 occur in the areas higher than 2950 m (the lower elevation limit of glacier coverage) while  
602 snowmelt can occur in areas higher than 1650 m. It can be deduced that snowmelt generally  
603 occurs at lower elevations than glacier melt. Remember that temperature decreases with  
604 increase in altitude. There should exist a period of time during which temperature at 1650 m is  
605 higher than snowmelt threshold while temperature above 2950 m is lower than glacier threshold  
606 and thus snowmelt does occur but glacier melt not.

607 The groundwater source should be a dominant source for the baseflow part of a hydrograph  
608 and, of course, it dominates the recession limb of a hydrograph (part of a baseflow partition)  
609 when no rainfall or melting occurs.

610 Based on the above physical understanding, we can partition the hydrograph using the  
611 following three indices:

612 (1) Date index ( $D_i$ ):  $D_i$  is used to distinguish the dates on which rainfall and thus possible  
613 rainwater directly runoff process occurs. For simplicity, in this study we use  $D_i$  to  
614 distinguish dry period and storm rain period and assume no rainfall runoff in the dry  
615 period, i.e.,

616 
$$D_i = \begin{cases} 1, & \text{for days in storm rain period from May to September} \\ 0, & \text{for days in relative dry period from October to April} \end{cases} \quad (3)$$

617 (2) Snowmelt index ( $S_i$ ):  $S_i$  indicates whether snowmelt possibly occurs on a given  
618 day:

619 
$$S_i = \begin{cases} 1, & \text{for days when temperature at altitude 1650 m is higher than } 0^\circ\text{C} \\ 0, & \text{for other days} \end{cases} \quad (4)$$

620 (3) Glacier melt index ( $G_i$ ):  $G_i$  is used to identify days when glacier melt possibly  
621 occurs:

622 
$$G_i = \begin{cases} 1, & \text{for days when temperature at altitude 2950 m is higher than } 0^\circ\text{C} \\ 0, & \text{for other days} \end{cases} \quad (5)$$

623 The hydrograph is then partitioned according to the three indices by using the following  
624 rules:

625 
$$Q = \begin{cases} Q_{SB} & \text{for } S_i=0, G_i=0, \text{ and } D_i = 0 \\ Q_{SB} + Q_{SM} & \text{for } S_i=1, G_i=0, \text{ and } D_i = 0 \\ Q_{SB} + Q_{SM} + Q_{GM} & \text{for } S_i=1, G_i=1, \text{ and } D_i = 0 \\ Q_{SB} + Q_{SM} + Q_{GM} + Q_R & \text{for } D_i = 1 \end{cases} \quad (6)$$

626 where,  $Q$  is the overall streamflow series,  $Q_{SB}$  stands for the baseflow generated by groundwater  
627 source,  $Q_{SM}$  for snow meltwater runoff,  $Q_{GM}$  for glacier meltwater runoff, and  $Q_R$  for rainwater  
628 directly runoff. The partitioning principles are described as follows:

629 (1) Groundwater is the dominant component ( $Q=Q_{SB}$ ) when both melt and rainwater  
630 directly runoff do not occur. This condition is mathematically equivalent to  $S_i+G_i+D_i=0$ , which  
631 requires  $S_i=0$ ,  $G_i=0$ , and  $D_i=0$ ;

632 (2) Snow meltwater and groundwater are the dominant components ( $Q=Q_{SB}+Q_{SM}$ ) when  
633 the temperature is higher than  $0^\circ\text{C}$  at 1650 m a.s.l. and lower than  $0^\circ\text{C}$  at 2950 m a.s.l.  
634 (requires  $S_i=1$ ,  $G_i=0$ , and  $D_i=0$ );

635 (3) Snow meltwater and glacier meltwater coupled with groundwater dominate  
636 ( $Q=Q_{SB}+Q_{SM}+Q_{GM}$ ) on days when the temperature at 2950 m a.s.l. exceeds  $0^\circ\text{C}$  in October to  
637 April. This means  $G_i=1$ ,  $D_i=0$ , and  $S_i=1$ , noting that  $S_i$  must be equal to 1 when  $G_i=1$  for the  
638 decreasing nature of temperature along altitude;

639 (4) Finally, all sources are mixed ( $Q=Q_{SB}+Q_{SM}+Q_{GM}+Q_R$ ) for other days in the storm rain



640 period (May to September,  $D_i=1$ ). Each category contains days that could be continuous or  
641 discontinuous in time and could lie within different weeks due to temporal variability of  
642 precipitation and temperature.

### 643 3.2 Tsinghua Representative Elementary Watershed Hydrological Model

644 The Tsinghua Representative Elementary Watershed model (THREW model) used for the  
645 hydrological simulation in this study, has been successfully applied in many watersheds in both  
646 China and the United States (see Tian *et al.*, 2008, 2012; Li *et al.*, 2012; Liu *et al.*, 2012 etc.),  
647 including an application to a high mountainous catchment of Urumqi River basin by Mou *et al.*  
648 (2008). The THREW model adopts the REW (Representative Elementary Watershed) approach  
649 to conceptualize a watershed, where REW is the sub-catchment unit for hydrological modeling.  
650 The study basin was divided into several units (REW) based on a digital elevation model. Sub-  
651 catchment units were further divided into a surface and sub-surface layer, each layer containing  
652 several sub-zones. The sub-surface layer is composed of two zones: saturated zone and  
653 unsaturated zone, and the surface layer consists of six zones: vegetated zone, bare soil zone,  
654 snow covered zone, glacier covered zone, sub-stream-network zone, and main channel reach;  
655 see Tian *et al.* (2006) for further details.

656 The main runoff generation processes simulated by the THREW model include rainfall  
657 surface runoff, groundwater baseflow, snowmelt and glacier melt. Rainfall surface runoff is  
658 simulated by a Xin'anjiang module, which adopts a water storage capacity curve to describe  
659 non-uniform distribution of water storage capacity of a sub-catchment (Zhao, 1992). The  
660 storage capacity curve is determined by two parameters (spatial averaged storage capacity  $W_M$   
661 and shape coefficient  $B$ ). Rainfall surface runoff forms on areas where storage is replete.  
662 Replete areas are calculated by the antecedent storage and current rainfall. The saturation excess  
663 runoff is computed based on water balance. The remainder of rainfall can infiltrate into soil and  
664 become additional contributions to groundwater. Groundwater forms baseflow that is  
665 separately calculated by two coefficients ( $K_A$  and  $K_D$ ).  $K_A$  and  $K_D$  are outflow coefficients of  
666 groundwater storage. Their sum determines the flow rate of groundwater baseflow and their  
667 ratio ( $K_D / K_A$ ) dominate the proportion of free groundwater storage. Infiltration and storage  
668 should have effects on the calibration of the two parameters. The Xin'anjiang module has been  
669 successfully applied to the Qiedeke, Kaidu, Manasi and Kahai basins in Tianshan Mountain by

670 different authors (Jiang, 1987; Yang *et al.*, 1987; Mu and Jiang, 2009), which indicates its  
671 applicability in our study area.

672 For the simulation of melt processes in this study, the THREW model was modified to  
673 couple with the temperature-index method, given the easy accessibility of air temperature data  
674 and generally good model performance of the temperature-index model (Hock, 2003; Singh *et al.*,  
675 2000). Snow and glacier melt are simulated using separate degree-day factors (snowmelt  
676 degree day factor  $D_s$  and glacier melt degree day factor  $D_g$ ). Glacier melt only occurs in glacier  
677 area according to CGI, which remains stable during the study period (2003-2012, see discussion  
678 in Sect. 2.2.3). Precipitation in the snow and glacier zone is divided into rainfall and snowfall  
679 according to two threshold temperature values ( $0^\circ\text{C}$  and  $2.5^\circ\text{C}$  are adopted in this study  
680 according to Wu and Li (2007)), i.e., when temperature is higher than  $2.5^\circ\text{C}$ , all precipitation  
681 is rainfall, when temperature is lower than  $0^\circ\text{C}$ , all precipitation is snowfall, and when  
682 temperature falls between the two thresholds, precipitation is divided into rainfall and snowfall  
683 half by half (a simple division scheme adopted here). Rainfall on glacier areas forms runoff and  
684 flows into the stream-network directly without infiltration into soil. Snow water equivalent  
685 (SWE) on glacier areas is updated by combining snowfall and snowmelt, and for simplicity,  
686 snow is assumed to cover all glacier areas when the corresponding SWE is not zero. Snowmelt  
687 in glacier areas is simulated using snow degree-day factor  $D_s$  until it melts away completely.  
688 Snow cover area in non-glacier area is updated using MODIS data. **To be noted, snowfall in**  
689 **each subcatchment is calculated according to the daily precipitation and temperature. And**  
690 **snowmelt is simulated using the degree-day method. However, the snow water equivalent in**  
691 **the snow cover zone (non-glacier area) is not computed. The existing of snow cover in each**  
692 **subcatchment is only determined by MODIS snow image. When the MODIS image indicates**  
693 **the existing of snow cover and meanwhile the daily temperature is higher than  $0^\circ\text{C}$ , then**  
694 **snowmelt will occur, otherwise, snowmelt will not occur. The identification of snow cover by**  
695 **MODIS image is in accordance with the fact that the partitioning of snowmelt dominant**  
696 **hydrograph is based on MODIS snow products. If the existing of snow cover is determined by**  
697 **snow water equivalent, the temperature parameters to calculate snowfall can have significant**  
698 **effects on the estimation of the degree-day factor for snowmelt. To partly reduce this effect, we**  
699 **calibrate the degree-day factor for snowmelt on the basis of MODIS snow cover products.**

700 Although in this way, the water balance of snow cover is not taken into account in the snow  
701 cover zone, it should not impact the calibration of the degree-day factor for snowmelt. Since  
702 MODIS SCA products (i.e., MYD10A2) are available from 2003, the model simulation period  
703 is from 2003 to 2012, of which 2003-2007 for calibration and 2008-2012 for evaluation. The  
704 time step for simulation is daily.

### 705 3.3 Stepwise Calibration of Grouped Parameters Upon Partitioning Curves

706 Model parameters are grouped *a priori* according to their connection with causal physical  
707 mechanisms (see Table 3). According to Xie *et al.* (2004) and Kang *et al.* (1980), parameters  
708 that control groundwater baseflow, snowmelt, glacier melt, and rainwater surface runoff should  
709 be the most sensitive parameters for the runoff simulation (also see our sensitivity analysis in  
710 Sect. 4.6). These parameters are subjected to calibration in this study. They are related to the  
711 corresponding hydrograph parts and then calibrated in a stepwise manner: first, groundwater  
712 baseflow parameters ( $K_A$  and  $K_D$ ) are estimated based on the  $Q_{SB}$  part of the hydrograph. Second,  
713 snowmelt degree day factor ( $D_s$ ) is calibrated upon the  $Q_{SB}+Q_{SM}$  part. Third, glacier melt  
714 degree-day factor ( $D_g$ ) is determined according to the  $Q_{SB}+Q_{SM}+Q_{GM}$  part. Finally, rainfall  
715 surface runoff parameters ( $B$ ,  $W_M$ ) are calibrated on days when  $D_i$  equals to 1, i.e., the  
716  $Q_{SB}+Q_{SM}+Q_{GM}+Q_R$  part of hydrograph.

717 In each step, only the specific parameter group is subjected to calibration. The parameters  
718 determined in the previous steps are kept constant, and all other parameters that will be  
719 calibrated in the next steps adopt their initial values. As the simulation in each step can, to some  
720 degree, be affected by the initial conditions produced in the preceding step, an iterative  
721 procedure is implemented to progressively minimize this influence. The parameter groups are  
722 first calibrated based on the corresponding hydrograph parts, and then the stepwise sequence is  
723 repeated until the calibrated parameters converge, i.e., the difference in parameter values  
724 between two contiguous iterations is less than 10%. In each calibration step, we use  $RMSE_{ln}$   
725 (Eqn. (7), emphasizing low flow) or  $RMSE$  (Eqn. (8), emphasizing high flow) as objective  
726 function for parameter optimization. The remaining, insensitive, parameters are determined *a*  
727 *priori* according to previous modeling experience (mainly from Sun *et al.* (2012)) and listed in  
728 Table 3. The initial values of the calibrated parameters are also determined *a priori* according  
729 to Sun *et al.* (2012) and Tian *et al.* (2012).

730 The overall streamflow can be simulated with all calibrated parameters, which is evaluated  
 731 with  $NSE$  and  $NSE \ln$  (logarithm Nash Criterion) values. Given that it is relatively easier to  
 732 obtain high evaluation merit values in snowmelt driven basins due to strong seasonality of  
 733 streamflow, we further adopt a simple benchmark model (the inter-annual mean value for every  
 734 calendar day) to evaluate performance of the proposed method by subtracting streamflow  
 735 seasonality. This benchmark model is proposed by Schaeffli and Gupta (2007) for basins having  
 736 a relatively constant seasonality. The improvement of a model comparing to the benchmark  
 737 model is quantified by the  $BE$ , see Eqn. (9) for detail.

$$738 \quad RMSE \ln = \sqrt{\frac{1}{n} \sum_{i=1}^n (\log Q_{obs}(i) - \log Q_{sim}(i))^2} \quad (7)$$

$$739 \quad RMSE = \sqrt{\frac{1}{n} \sum_{i=1}^n (Q_{obs}(i) - Q_{sim}(i))^2} \quad (8)$$

$$740 \quad BE = 1 - \frac{\sum_{i=1}^n (Q_{obs}(i) - Q_{sim}(i))^2}{\sum_{i=1}^n (Q_{obs}(i) - Q_{ben}(i))^2} \quad (9)$$

## 741 4 Results and Discussion

### 742 4.1 Partitioning Hydrographic Curves

743 The hydrograph from 2003 to 2012 was partitioned based on Eqn. (6). In total, we obtained  
 744 four kinds of partitioning curves, i.e.  $Q_{SB}$  part,  $Q_{SB}+Q_{SM}$  part,  $Q_{SB}+Q_{SM}+Q_{GM}$  part and  
 745  $Q_{SB}+Q_{SM}+Q_{GM}+Q_R$  part. As an example, the partitioning curves in 2003 are shown in Fig. 6, in  
 746 which the melting period ranges from late February to late November (labeled as red and green  
 747 dots). Snowmelt (red dots) starts in February and ends in November, while glacier melt (green  
 748 dots) starts later (March) and stops earlier (October). This melt situation agrees well with the  
 749 previous studies of Kang *et al.* (1980) and Sun *et al.* (2012). Hydrograph parts dominated by  
 750 groundwater source mainly fall into December, January and February and are denoted by black  
 751 dots. The rainwater surface runoff occurs in the storm rain period only (May to September,  
 752 denoted by blue dots). The total number of days of  $Q_{SB}+Q_{SM}$  part from 2003 to 2007 is 365,  
 753 and that of  $Q_{SB}+Q_{SM}+Q_{GM}$  part is 249, while the  $Q_{SB}+Q_{SM}+Q_{GM}+Q_R$  part occupies 765 days.  
 754 The numbers of non-melt days (i.e. the  $Q_{SB}$  part, due to glacier melt generally occurs in the  
 755  $Q_{SB}+Q_{SM}+Q_{GM}+Q_R$  part) in the five years are 114, 80, 89, 96, and 68, respectively.

756 Correspondingly, the mean temperatures in those years gauged at the THS are 8.9, 10.1, 9.9,  
757 10.4, and 11.3°C, respectively. A lower mean annual temperature causes a longer non-melt  
758 period in that year and vice versa. Note that the partitioning curves can be discontinuous in time  
759 due to the spatial-temporal variability of temperature.

#### 760 **4.2 Model Calibration by the Stepwise Method**

761 The six key parameters ( $K_A$ ,  $K_D$ ,  $D_s$ ,  $D_g$ ,  $W_M$ , and  $B$ ) were firstly calibrated by the proposed  
762 stepwise and iterative method. To focus on baseflow generated by the groundwater source  
763 during the  $Q_{SB}$  period, the  $RMSEln$  metric that emphasizes low flow is chosen as the evaluation  
764 criterion for the calibration of parameters  $K_A$  and  $K_D$ . Conversely, high flow is our focus for  
765 the remaining periods ( $Q_{SB}+Q_{SM}$ ,  $Q_{SB}+Q_{SM}+Q_{GM}$ ,  $Q_{SB}+Q_{SM}+Q_{GM}+Q_R$ ) and the  $RMSE$  metric is  
766 chosen as the evaluation criterion for calibration of parameters  $D_s$ ,  $D_g$ , and  $W_M$  and  $B$ . To deal  
767 with interaction between steps, an iterative calibration approach was adopted. A total of five  
768 iterations was implemented until the parameter estimates became stable; the simulation of each  
769 kind of partitioning curve in each step of the last iteration is presented in Fig. 7. The calibrated  
770 parameters are shown in Table 4 and the evaluation merits are listed in Table 5.

771 Figure 7a shows that the magnitude of baseflow in  $Q_{SB}$  part was captured well at most of  
772 the times. The  $RMSEln$  merit is 0.302 m<sup>3</sup>/s, and the parameters  $K_A$  and  $K_D$  were determined as  
773 1.1 and 0.002 respectively. Streamflow in the  $Q_{SB}+Q_{SM}$  part is dominated by both snow  
774 meltwater and groundwater. The Fig.7b shows that melt peak flow events have also been  
775 captured well by a calibrated  $D_s$  as 2.5 mm °C<sup>-1</sup> day<sup>-1</sup> after the determination of  $K_A$  and  $K_D$  in  
776 the first step. For the  $Q_{SB}+Q_{SM}+Q_{GM}$  part, glacier meltwater began to control the streamflow in  
777 combination with snow meltwater and groundwater. Snowmelt and baseflow were determined  
778 *a priori* by previously calibrated parameters. The remaining residual between the simulated and  
779 observed discharge can be attributed to glacier melt alone, which was thus used for the  
780 calibration of glacier melt factor  $D_g$ . The  $RMSE$  value for this hydrograph partition was  
781 optimized as 4.784 m<sup>3</sup>/s and we obtained a sound simulation by a calibrated  $D_g$  as 7.2 mm °C<sup>-1</sup>  
782 day<sup>-1</sup> as shown in Fig.7c. During the storm rain periods ( $Q_{SB}+Q_{SM}+Q_{GM} +Q_R$  part), rainwater  
783 directly runoff is an additional important component of river runoff. Similarly, parameters  $W_M$   
784 and  $B$  can be calibrated separately after *a priori* determination of melt runoff and groundwater  
785 baseflow. The simulated  $RMSE$  value in this period is 12.650 m<sup>3</sup>/s, with calibrated  $W_M=10.50$ cm

786 and  $B=0.80$ . The overall daily streamflow simulation is obtained by combining the four  
787 partitions together (see Figure 8a). The corresponding  $NSE$  index is 0.881 and  $NSEln$  is 0.929.  
788 Generally the results suggest a sound simulation compared to the observation.

789 To be noted, the calibrated values of melt degree day factors  $D_s$  ( $2.5\text{mm } ^\circ\text{C}^{-1} \text{ day}^{-1}$ ) and  $D_g$   
790 ( $7.2\text{mm } ^\circ\text{C}^{-1} \text{ day}^{-1}$ ) are similar to the values obtained in other studies in Tainshan area, e.g.,  $D_s$   
791 is calibrated as  $2.5 \text{ mm } ^\circ\text{C}^{-1} \text{ day}^{-1}$  by Liu *et al.* (2012), and  $D_s$  and  $D_g$  are estimated as  $3.1 \text{ mm } ^\circ\text{C}^{-1}$   
792  $\text{ day}^{-1}$  and  $7.3 \text{ mm } ^\circ\text{C}^{-1} \text{ day}^{-1}$  respectively based on observed mass balance data by Liu *et al.*  
793 (1999), which indicates the robustness of our calibration method.

#### 794 **4.3 Comparison to Automatic Calibration Method**

795 For comparison, we also carry out an automatic calibration with the help of the  $\varepsilon$ -NSGAI  
796 algorithm, an optimization method developed by Deb *et al.* (2002) and Kollat and Reed (2006).  
797 The six parameters were calibrated together and evaluated by  $NSE$  value of the overall  
798 hydrograph. The run time of the automatic algorithm is about 5 weeks (840 hour on a desktop  
799 equipped with an Intel Core i7 CPU with 2.8GHz). The  $NSE$  value for the final optimized  
800 parameters is 0.868, and the  $NSEln$  value is 0.846 (Fig. 8b), both of which are lower than the  
801 values obtained by the proposed stepwise method. The parameters calibrated by  $\varepsilon$ -NSGAI are  
802 listed in Table 4, and are different from those calibrated by the stepwise method. Specifically,  
803 the snowmelt degree-day factor ( $D_s$ ) and groundwater baseflow parameters ( $K_A$  and  $K_D$ )  
804 obtained by  $\varepsilon$ -NSGAI are  $2.03\text{mm } ^\circ\text{C}^{-1} \text{ day}^{-1}$  and 5.6 and 99.1 respectively. The evaluation  
805 merits of  $RMSE$  and  $RMSEln$  for each partitioning curve are also shown in Table 5. In general,  
806 the simulation by the automatic algorithm is not as good as that by the stepwise method,  
807 especially for the low and middle flow partitions ( $Q_{SB}+Q_{SM}$  and  $Q_{SB}+Q_{SM}+Q_{GM}$ ). This may be  
808 due to the tendency of NSE-based automatic calibration to emphasize high flows.

809 To make a further evaluation, a benchmark model suggested by Schaepli and Gupta (2007)  
810 is used for the comparison, which simply simulates daily runoff as the inter-annual daily mean  
811 value. Simulation results by the benchmark model are shown in the Figure 8c, which shows  
812  $NSE$  value as 0.815 and  $NSEln$  value as 0.923. The high  $NSE$  and  $NSEln$  values can be attributed  
813 to the strong seasonality of stream discharge in the study basin (Schaepli and Gupta, 2007). The  
814  $BE$  index (Eqn. (9), see Table 5) is used to measure the improvement of simulations by the  
815 calibration methods compared to the benchmark model. A positive value for  $BE$  means that the

816 evaluated method outperforms the benchmark model. Figure 8 shows the simulations of daily  
817 streamflow by the three methods (Fig.8a by stepwise calibration method, Fig.8b by automatic  
818 calibration method and Fig.8c by benchmark model), which shows better simulation by the two  
819 calibration runs with THREW model than the benchmark model (*BE* values are both positive).  
820 The stepwise calibration run obtained a *BE* value of 0.355, while *BE* of the automatic calibration  
821 run is 0.271. The benchmark model describes the mean value of daily discharge on each  
822 calendar day. The higher the *BE* value is, the better the seasonal variability of the hydrograph  
823 is captured by the evaluation method. The higher *BE* value in the stepwise calibration method  
824 can be attributed to the better simulation of middle and low flows which are dominated by  
825 groundwater and melt water (Fig.8a). However, *BE* values simulated by two calibrated  
826 parameter sets are both relatively low, which is attributed to the poor mimic of the (rapidly  
827 rising and falling) peaks.

828 Note that the automatic calibration method based on *NSE* value of the overall hydrograph  
829 adopts 1D measurement information to optimize four parameter groups. **Benefitting from the**  
830 **partitioning curves, however, the stepwise calibration method increases the dimension of**  
831 **hydrological signature to four. The signature dimension is now equal to the number of**  
832 **parameter groups**, and the grouped parameters can be optimized according to their  
833 corresponding runoff sources separately. A sound simulation of the overall hydrograph is  
834 obtained by the reasonable reproduction of the separate partitioning curves. Therefore,  
835 parameters calibrated by the stepwise method are inclined to have more explicit physical basis.

836 In regards to computation efficiency, the stepwise calibration required 385 runs of the  
837 model to complete, with each model run taking about 1.5 minutes and the total computation  
838 time being about 10 hrs. In contrast, the state-of-the-art automatic calibration algorithm  
839 required about 5 weeks of CPU time consumption on a desktop equipped with an Intel Core i7  
840 CPU and 2.8GHz. The comparison indicates that the stepwise calibration method is both more  
841 physically based as well as more computationally efficient.

842 **It is worth noting, the performance of the automatic calibration algorithm can increase if**  
843 **the algorithm keeps on running, and even be higher than that of the step-wise calibration method.**  
844 **The comparison here is intending to show that the step-wise calibration method based on**  
845 **hydrograph partition can achieve considerable performance more effectively. The automatic**

846 algorithm here treats all the parameters equally during the calibration period. Each parameter  
847 should be optimized when searching for the optimal parameter set. This searching algorithm  
848 hampers the efficiency of the calibration procedure without identifying the dominant sub-  
849 periods for different parameters. In the step-wise calibration method, only parameters that are  
850 responsible for the simulation of corresponding hydrograph partition are optimized in each step.  
851 And also the calibration of parameter by this method reflects the role of each parameter for the  
852 basin runoff generation.

#### 853 4.4 Evaluation for the Stepwise Calibration Method

854 The parameter set calibrated by the stepwise method is applied to the evaluation period  
855 (2008~2012), and the daily discharge simulation is shown in Fig.9a. The evaluation merits are  
856 listed in Table 5. The *NSE*, *NSEln* and *RMSE* values for the whole period indicate sound  
857 evaluation results but general lower performance compared to calibration period. However, the  
858 evaluation results by the stepwise method are still significant better than the benchmark model,  
859 which obtained a *NSE* value as low as 0.577 (Fig. 9b and Table 5). The *BE* value in evaluation  
860 period by the stepwise calibration method is 0.413. Furthermore, from the partition perspective,  
861 the *RMSEln* and *RMSE* values for four partitions in Table 5 show that the low flow simulations  
862 ( $Q_{SB}$ ,  $Q_{SB}+Q_{SM}$ , and  $Q_{SB}+Q_{SM}+Q_{GM}$  parts) are pretty good and even outperform the calibration  
863 simulations. The high flow simulation ( $Q_{SB}+Q_{SM}+Q_{GM}+Q_R$  part) is, however, insufficient, with  
864 *RMSE* 16.727m<sup>3</sup>/s (compared to 12.65 m<sup>3</sup>/s in calibration period). The lower performance of  
865 overall evaluation should be attributed to the insufficiency in storm rain days, especially for  
866 some extreme storm events in the summer of 2010 (see Fig. 9a). The underestimation of these  
867 events is likely due to inadequate observations of rainfall, which are principally due to the  
868 strong spatial variability of rainfall in mountainous areas. It is widely acknowledged that the  
869 extreme runoff events are difficult to capture in mountain area, where gauged station is scarce,  
870 on the daily scale (Aizen *et al.*, 2000; Jasper *et al.*, 2002). However, the accuracy of our results  
871 is similar to Li and Williams (2008) (used SRM model) and Liu *et al.*(2012) (who used the  
872 MIKE-SHE model) who performed similar work in a basin that is close to TRB in Tianshan  
873 Mountains. Their Nash values for daily discharge varied from 0.51 to 0.78, and also failed to  
874 simulate the peak flows in summer. They also attributed the low efficiency to the heavy  
875 precipitation.



876 To further evaluate the robustness of the stepwise calibration method based on partitioning  
877 curves, cross validation was implemented. The hydrograph in the evaluation period was  
878 partitioned based on dominant runoff sources, as was done in the calibration years 2003-2007.  
879 We calibrated the model to 2008-2012 and evaluated it for 2003-2007. The new calibrated  
880 parameter values are  $K_A=0.9$ ,  $K_D=0.003$ ,  $D_s=2.2 \text{ mm } ^\circ\text{C}^{-1} \text{ day}^{-1}$ ,  $D_g=7.4 \text{ mm } ^\circ\text{C}^{-1} \text{ day}^{-1}$ ,  
881  $W_M=10.2\text{cm}$  and  $B=0.77$ , which are similar to the values calibrated in 2003-2007 listed in Table  
882 4. The *NSE*, *NSEln* and *RMSE* values for calibration period 2008-2012 and evaluation period  
883 2003-2007 are 0.757, 0.900, 10.892m<sup>3</sup>/s and 0.883, 0.910, 8.589m<sup>3</sup>/s, respectively, using this  
884 new calibrated parameter set. The simulations of the two periods by cross validation are  
885 presented in Fig.9c-d, which shows similar performance by two calibrated parameter sets and  
886 further demonstrates the robustness of the proposed stepwise calibration method.

#### 887 **4.5 Sensitivity Analysis on Index-based Partitioning Method**

888 The stepwise calibration method relies heavily on the hydrograph partition for different  
889 runoff sources. The indices defined in Sect. 3.1 are keys to identify the dominant days for melt  
890 water and rainwater. The definitions for elevation bands for the 0 °C Isotherm and for storm rain  
891 days in the year producing rainwater runoff should have significant influence on the parameter  
892 calibration. In this study, the elevation band of 0 °C Isotherm for snowmelt is fixed and defined  
893 as 1650m. This value should have minimal effect on the snowmelt simulation, as the occurrence  
894 of snowmelt is actually determined by the MODIS snow cover data. Glacier cover area is  
895 assumed as constant, which is very rough for we have only one CGI data. In this section, we  
896 define different elevation bands of 0 °C Isotherm for glacier to analyze the effect of glacier area  
897 variation on the model calibration. We also select different seasons as the storm rain period to  
898 analyze its sensitive effect.

899 According to the CGI data, the glacier area extends from the altitude of 2950m in 2002.  
900 Considering the possible variability, we define four different lowest elevation bands for the  
901 glacier area (LEG), i.e., -500m (2450m), -200m (2750m), +200m (3150m) and +500m (3450m).  
902 As an example, various hydrograph partition patterns in year 2003 are shown in Fig. 10. For  
903 the storm rain period (SRP), new seasons are defined as April to October, April to September,  
904 May to October, and June to August compared to the benchmark period May to September. A  
905 new hydrograph partition pattern in year 2003 is also shown in Fig. 10. The left column in Fig.

906 10 shows that the  $Q_{SB}+Q_{SM}+Q_{GM}$  partition becomes longer while the  $Q_{SB}+Q_{SM}$  partition  
907 becomes shorter when the LEG is lower. Therefore, glacier melt starts earlier and ends later in  
908 the years with lower LEG. In the right column, the  $Q_{SB}+Q_{SM}+Q_{GM}$  partition becomes longer  
909 with the shorter SRP, while the variation of the  $Q_{SB}+Q_{SM}$  partition can be negligible. Parameters  
910 were re-calibrated according to the new partition curves, and the results are shown in Table 6,  
911 indicating the increase of degree-day factor for glacier melt ( $D_g$ ) with the increase of the LEG.  
912 The value of  $D_g$  is also found to become higher when the SRP falls in the warmer months. The  
913 variation of LEG imposes significant impacts on the calibration of  $D_g$ , with a result ranging  
914 from 5.8 to 8.0mm °C<sup>-1</sup> day<sup>-1</sup>, while the variation of SRP principally impacts the calibration of  
915 parameter  $W_M$ , with a result ranging from 8.2 to 10.5cm. However, the *NSE* values (see Table  
916 6) for different settings show minimal differences. This can be attributed to the fact that  
917 parameters are optimized on separate partitioning curves in the stepwise calibration method.  
918 Each hydrograph partition can be well simulated by adjusting the parameter values. The  
919 partition patterns can influence the value of parameters significantly but only slightly influence  
920 the discharge simulation. Among various LEGs, the setting of 2950m leads to the highest *NSE*  
921 value. Glacier melt degree day factor ( $D_g$ ) calibrated with this LEG is 7.2 mm °C<sup>-1</sup> day<sup>-1</sup>, which  
922 is very close to the value estimated as 7.3 mm °C<sup>-1</sup> day<sup>-1</sup> by Liu *et al.*(1999), in which the  $D_g$  is  
923 estimated according to the observed glacier mass balance data in Tianshan area. This can further  
924 demonstrate the reasonability of the assumption in Sect. 3.2 that the glacier area is stable and  
925 its lowest elevation is fixed at 2950m during the study period. For the various storm rain periods  
926 (SRP), when the May to October period is adopted, the discharge simulation is slightly better  
927 than the benchmark setting of SRP, i.e. May to September. This phenomenon seems to indicate  
928 the importance of precipitation measurement as discussed in Sect. 4.4. With the help of more  
929 advanced precipitation measurement, the storm rain period can be determined more precisely  
930 to improve the model simulation.

931 To evaluate the relative dominance of multiple runoff sources on the total runoff, we  
932 compute their contributions to total runoff by various LEG and SRP in Fig.11. The mean  
933 contributions of every runoff source are as follows: groundwater contributes 17%, snow  
934 meltwater contributes 16.5%, glacier meltwater contributes 40% and rainwater directly runoff  
935 contributes 26.5%. Total melt water (snowmelt and glacier melt) occupies approximately 56.5%

936 and is close to the ratio 63% suggested by Kang *et al.* (1980).

#### 937 **4.6 Sensitivity Analysis on Parameters**

938 The number of parameters to be calibrated is determined by the parameter sensitivity and  
939 *a priori* analysis. To evaluate the effect of different parameters on the simulation of different  
940 hydrograph partitions, we implemented a simple parameter sensitivity procedure that is carried  
941 out by a “one-at-a-time” approach. Parameters from different groups in Table 3 are selected for  
942 sensitivity analysis, including saturated hydraulic conductivity for u-zone  $K_s^u$ , saturated  
943 hydraulic conductivity for s-zone  $K_s^s$ , subsurface flow coefficient  $K_A$  and  $K_D$ , manning  
944 roughness coefficient for hillslope  $n^l$ , spatial heterogeneous coefficient for infiltration capacity  
945  $\alpha^{FL}$ , ground surface depression storage capacity  $Fmax^b$ , shape coefficient to calculate the  
946 saturation excess runoff area from the Xin’anjiang model  $B$ , spatial averaged tension water  
947 storage capacity in the Xin’anjiang model  $W_M$ , glacier degree day factor  $D_g$  and snowmelt  
948 degree per day factor  $D_s$ . Parameter are varied from -50% to +50% of the calibrated values  
949 using the stepwise method in Table 4. The relative change ( $R_{MS}$ ) of simulated measure merits  
950 ( $RMSEln$  or  $RMSE$ ) for different hydrograph partitions are used to evaluate the sensitivity (Eqn.  
951 (10)), where  $MS$  is the value of measure merits by the calibrated parameter,  $MS_+$  is the merits  
952 value obtained by the parameter +50% of the calibrated one, and  $MS_-$  is the merits value  
953 obtained by the parameter -50% of the calibrated one. The sensitivity simulation results are  
954 shown in Table 7, which demonstrates the dominant control of parameter  $K_A$ ,  $K_D$ ,  $W_M$ ,  $B$ ,  $D_s$  and  
955  $D_g$ . Some parameters have significant effects on simulation of multi hydrograph partitions. For  
956 example, parameters controlling the  $Q_{SB}+Q_{SM}+Q_{GM}+Q_R$  period can also have significant effect  
957 on the other periods. To minimize this interaction, iterative calibration was implemented in the  
958 calibration procedure. The number of calibrated parameters is determined as six, which control  
959 the main runoff sources (i.e. groundwater baseflow, snowmelt, glacier melt and rainwater  
960 directly runoff). Note that the low dimension of parameter calibration should not account for  
961 the low efficiency of peak flow simulation, referring to the similar study in Tianshan mountain  
962 areas by Li and Williams (2008), and Liu *et al.*(2012), in which the models have a higher  
963 parameter dimension (higher than six), and the peak flow simulations are still inadequate.

$$964 \quad R_{MS} = \left| \frac{MS_+ - MS_-}{MS} \right| \times 100\% \quad (10)$$

## 965 **5 Summary and Conclusion**

966 This study proposes diagnostic calibration approach to extracting **hydrological signatures**  
967 from available data series in a mountain area, which can be further used to partition the  
968 hydrograph into dominant runoff sources. The parameters of a hydrological model were  
969 grouped according to runoff sources and then related to the corresponding hydrologic  
970 partitioning curve. Each parameter group was calibrated to improve the simulation of the  
971 corresponding partitioning curve in a stepwise way. In this way, the dimension of **hydrological**  
972 **signature** is expanded to equal the number of parameter groups. The parameter uncertainty due  
973 to interaction of parameters is reduced via an iterative calibration procedure. Application to a  
974 mountain watershed in the Tianshan Mountain in northwestern China showed that the approach  
975 performed reasonably well. Cross validation and comparison to an automatic calibration  
976 method indicated its applicability.

977 Note that a semi-distributed hydrological model was utilized to illustrate the proposed  
978 diagnostic calibration approach in the high mountainous Tailan River Basin. Glacier mass  
979 balance is not simulated in the model and the glacier coverage was kept fixed during the study  
980 period, which can be subject to significant change in the context of global warming. According  
981 to existing studies (Stahl *et al.*, 2008; Schaefli and Huss, 2011; Jost *et al.*, 2012), glacier mass  
982 balance data is useful to constrain the parameter uncertainty for hydrological modeling in a  
983 glaciated basin. While arguing that our assumption of unchanged glacier coverage will not  
984 weaken the importance of the proposed approach, we acknowledge that an improved model  
985 coupled with glacier mass balance equations will improve the accuracy of hydrological  
986 simulation aided by glacier mass balance observations. This is left for future research.

987 A prerequisite for the proposed approach is hydrograph partitioning based on dominant  
988 runoff sources. The key to the partition procedure is to identify the functional domain of each  
989 runoff source from signature information extracted from easily available data. A partition can  
990 be achieved in which the relative roles of different runoff sources in the basin runoff vary  
991 significantly with time. The mountain watershed is an area in which the runoff sources can be  
992 separated by the combination of topography, ground-gauged temperature and precipitation, and  
993 remotely sensed snow and glacier coverage. Other areas with strong temporal variability of  
994 catchment wetness along with precipitation (e.g., monsoon zones) could also be suitable for the

995 proposed approach. The Dunne runoff is prone to dominate the hydrograph when the catchment  
996 is wet and it could switch to Hortonian runoff rapidly under the combination of high evaporative  
997 demand and less precipitation, as shown by Tian *et al.* (2012) in the Blue River basin of  
998 Oklahoma. This is, however, also left for future research.

999 *Acknowledgments.* We wish to thank Mr. Wang Xinhui for his assistance in collecting  
1000 hydrometeorology data in the Tailan River basin, and thank Charlie Luce and Viviana Lopez-  
1001 Burgos who provided great help in MODIS snow coverage product filtering. The authors would  
1002 also like to thank sincerely two Referees (B. Schafli and M. Zappa) and Editor Markus Weiler  
1003 for his careful comments, which improve the quality of manuscript significantly. This study  
1004 was supported by the National Science Foundation of China (NSFC 51190092, U1202232,  
1005 51222901) and the foundation of the State Key Laboratory of Hydroscience and Engineering  
1006 of Tsinghua University (2012-KY-03, 2014-KY-01). Their support is greatly appreciated.

1007 **References**

- 1008 Ackerman, S. A., Strabala, K. I., Menzel, W. P., Frey, R. A., Moeller, C. C. and Gumley, L. E.:  
1009 Discriminating clear sky from clouds with MODIS, *J. Geophys. Res.*,103, 32141-32157,  
1010 1998.
- 1011 Aizen, V., Aizen, E., Glazirin, G. and Loaiciga, H. A.: Simulation of daily runoff in Central  
1012 Asian alpine watersheds, *J. Hydrol.*, 238, 15-34, 2000.
- 1013 Akyurek, Z., Surer, S. and Beser, O.: Investigation of the snow-cover dynamics in the Upper  
1014 Euphrates Basin of Turkey using remotely sensed snow-cover products and  
1015 hydrometeorological data, *Hydrol. Process.*,25 (23), 3637-3648, 2011.
- 1016 Arnold, J. G. and Allen, P. M.: Automated methods for estimating baseflow and ground water  
1017 recharge from streamflow records, *Journal of the American Water Resources Association*,  
1018 35, 411-424, 1999.
- 1019 Arnold, J. G., Allen, P. M., Muttiah, R. and Bernhardt, G.: Automated base-flow separation and  
1020 recession analysis techniques, *Ground Water*, 33, 1010-1018, 1995.
- 1021 Beven, K.: Prophecy, reality and uncertainty in distributed hydrological modelling, *Adv. Water*  
1022 *Resour.*, 16, 41-51, 1993.
- 1023 Beven, K.: Equifinality and uncertainty in geomorphological modelling, *The Scientific Nature*  
1024 *of Geomorphology: Proceedings of the 27th Binghamton Symposium in Geomorphology*,  
1025 289-313, 1996.
- 1026 Beven, K. and Binley, A.: The future of distributed models-model calibration and uncertainty  
1027 prediction, *Hydrol. Process.*, 6, 279-298, 1992.
- 1028 Beven, K. and Freer, J.: Equifinality, data assimilation, and uncertainty estimation in  
1029 mechanistic modelling of complex environmental systems using the GLUE methodology, *J.*  
1030 *Hydrol.*,249, 11-29, 2001.
- 1031 Blöschl, G., Sivapalan, M., Wagener, T., Viglione, A. and Savenije, H.(Eds.): *Runoff*  
1032 *Prediction in Ungauged Basins: Synthesis Across Processes, Places and Scales*, Cambridge  
1033 *Univ. Press*, New York,2013.
- 1034 Boyle, D. P., Gupta, H. V. and Sorooshian, S.: Toward improved calibration of hydrologic  
1035 models: Combining the strengths of manual and automatic methods, *Water Resour. Res.*, 36,  
1036 3663-3674, 2000.
- 1037 Brazil, L.: Multilevel calibration strategy for complex hydrologic simulation models, NOAA  
1038 *Technical Report*, NWS 42, Fort Collins, 217 pp, 1989.
- 1039 Bulygina, N., McIntyre, N. and Wheeler, H.: Conditioning rainfall-runoff model parameters for  
1040 ungauged catchments and land management impacts analysis, *Hydrol. Earth Syst. Sci.*, 13  
1041 (6), 893-904, 2009.
- 1042 Daly, S. F., Davis, R., Ochs, E. and Pangburn, T.: An approach to spatially distributed snow  
1043 modelling of the Sacramento and San Joaquin basins, California, *Hydrol. Process*, 14 (18SI),  
1044 3257-3271, 2000.
- 1045 Deb, K., Pratap, A., Agarwal, S. and Meyarivan, T.: A fast and elitist multiobjective genetic  
1046 algorithm: NSGA-II, *IEEE Transactions on evolutionary computation*, 6, 182-197, 2002.
- 1047 Detenbeck, N. E., Brady, V. J., Taylor, D. L., Snarski, V. M. and Batterman, S. L.: Relationship  
1048 of stream flow regime in the western Lake Superior basin to watershed type characteristics,  
1049 *J. Hydrol.*, 309, 258-276, 2005.
- 1050 Duan, Q., Sorooshian, S. and Gupta, V.: Effective and efficient global optimization for

1051 conceptual rainfall-runoff models, *Water Resour. Res.*, 28, 1015-1031, 1992.

1052 Dunn, S. M. and Colohan, R. J. E.: Developing the snow component of a distributed  
1053 hydrological model: a step-wise approach based on multi-objective analysis, *J. Hydrol.*, 223,  
1054 1-16, 1999.

1055 Eder, G., Fuchs, M., Nachtnebel, H. and Loibl, W.: Semi-distributed modelling of the monthly  
1056 water balance in an alpine catchment, *Hydrol. Process.*, 19, 2339-2360, 2005.

1057 Farmer, D., Sivapalan, M. and Jothityangkoon, C.: Climate, soil, and vegetation controls upon  
1058 the variability of water balance in temperate and semiarid landscapes: Downward approach  
1059 to water balance analysis, *Water Resour. Res.*, 39, 1035, 2003.

1060 Fierz, C., Ribet, P., Adams, E., Curran, A., Fohn, P., Lehning, M. and Pluss, C.: Evaluation of  
1061 snow-surface energy balance models in alpine terrain, *J. Hydrol.*, 282 (1-4), 76-94, 2003.

1062 Gafurov, A. and Bardossy, A.: Cloud removal methodology from MODIS snow cover product,  
1063 *Hydrol. Earth Syst. Sci.*, 13, 1361-1373, 2009.

1064 Gan, T. Y. and Biftu, G. F.: Automatic calibration of conceptual rainfall-runoff models:  
1065 Optimization algorithms, catchment conditions, and model structure, *Water Resour. Res.*, 32,  
1066 3513-3524, 1996.

1067 Gao, W., Li, Z. and Zhang, M.: Study on Particle-size Properties of Suspended Load in Glacier  
1068 Runoff from the Tomor Peak, *Arid Zone Research*, 28, 449-454, 2011(in Chinese).

1069 Gomez-Landesa, E. and Rango, A.: Operational snowmelt runoff forecasting in the Spanish  
1070 Pyrenees using the snowmelt runoff model, *Hydrol. Process.*, 16, 1583-1591, 2002.

1071 Gupta, H. V., Kling, H., Yilmaz, K. K. and Martinez, G. F.: Decomposition of the mean squared  
1072 error and NSE performance criteria: Implications for improving hydrological modelling, *J.*  
1073 *Hydrol.*, 377, 80-91, 2009.

1074 Gupta, H. V., Sorooshian, S. and Yapo, P. O.: Toward improved calibration of hydrologic  
1075 models: Multiple and noncommensurable measures of information, *Water Resour. Res.*, 34,  
1076 751-763, 1998.

1077 Gupta, V. K. and Sorooshian, S.: Uniqueness and observability of conceptual rainfall-runoff  
1078 model parameters: The percolation process examined, *Water Resour. Res.*, 19, 269-276,  
1079 1983.

1080 Gupta, V. K. and Sorooshian, S.: The Automatic Calibration of Conceptual Catchment Models  
1081 Using Derivative-Based Optimization Algorithms, *Water Resour. Res.*, 21, 437-485, 1985.

1082 Gupta, H. V., Wagener, T. and Liu, Y.: Reconciling theory with observations: elements of a  
1083 diagnostic approach to model evaluation, *Hydrol. Process.*, 22, 3802-3813, 2008.

1084 Gurtz, J., Baltensweiler, A. and Lang, H.: Spatially distributed hydrotope-based modelling of  
1085 evapotranspiration and runoff in mountainous basins, *Hydrol. Process.*, 13, 2751-2768, 1999.

1086 Haberlandt, U., Klocking, B., Krysanova, V. and Becker, A.: Regionalisation of the base flow  
1087 index from dynamically simulated flow components - a case study in the Elbe River Basin,  
1088 *J. Hydrol.*, 248, 35-53, 2001.

1089 Hingray, B., Schaepli, B., Mezghani, A. and Hamdi, Y.: Signature-based model calibration for  
1090 hydrological prediction in mesoscale Alpine catchments, *Hydrolog. Sci. J.*, 55 (6), 1002-  
1091 1016, 2010.

1092 Hock, R.: Temperature index melt modelling in mountain areas, *J. Hydrol.*, 282, 104-115, 2003.

1093 Hooper, R. P. and Shoemaker, C. A.: A Comparison of Chemical and Isotopic Hydrograph  
1094 Separation, *Water Resour. Res.*, 22, 1444-1454, 1986.



1095 Howard, C.: Revisiting the degree-day method for snowmelt computations – Discussion, *Water*  
1096 *Resources Bulletin*, 32 (2), 411-413, 1996.

1097 Huss, M., Farinotti, D., Bauder, A. and Funk, M.: Modelling runoff from highly glacierized  
1098 alpine drainage basins in a changing climate, *Hydrol. Process.*, 22 (19SI), 3888-3902, 2008.

1099 Jasper, K., Gurtz, J. and Herbert, L.: Advanced flood forecasting in Alpine watersheds by  
1100 coupling meteorological observations and forecasts with a distributed hydrological model, *J.*  
1101 *Hydrol.*, 267 (1-2), 40-52, 2002.

1102 Jiang, H. F.: Snow ablation modeling and its application to Qiedeke basin, *Journal of Xinjiang*  
1103 *Agricultural University*, 1, 67-75, 1987 (in Chinese).

1104 Johnston, P. R. and Pilgrim, D. H.: Parameter optimization for watershed models, *Water Resour.*  
1105 *Res.*, 12, 477-486, 1976.

1106 Jost, G., Moore, R. D., Menounos, B. and Wheate, R.: Quantifying the contribution of glacier  
1107 runoff to streamflow in the upper Columbia River Basin, Canada, *Hydrol. Earth Syst.*  
1108 *Sci.*, 16, 849-860, 2012.

1109 Jothityangkoon, C., Sivapalan, M. and Farmer, D. L.: Process controls of water balance  
1110 variability in a large semi-arid catchment: downward approach to hydrological model  
1111 development, *J. Hydrol.*, 254, 174-198, 2001.

1112 Juston, J., Seibert, J. and Johansson, P.: Temporal sampling strategies and uncertainty in  
1113 calibrating a conceptual hydrological model for a small boreal catchment, *Hydrol.*  
1114 *Process.*, 23 (21), 3093-3109, 2009.

1115 Kane, D. L., Gieck, R. E., and Hinzman, L. D.: Snow Modeling at Small Alaskan Arctic  
1116 Watershed, *Journal of Hydrologic Engineering*, 2 (4), 204-210, 1997.

1117 Kang, E., Zhu, S. and Huang, M.: Some Results of the Research on Glacial Hydrology in the  
1118 Region of MT. Tuomuer, *Journal of Glaciology and Geocryology*, 2, 18-21, 1980 (in  
1119 Chinese).

1120 Klok, E. J., Jasper, K., Roelofsma, K. P., Gurtz, J. and Badoux, A.: Distributed hydrological  
1121 modelling of a heavily glaciated Alpine river basin, *Hydrolog. Sci. J.*, 46 (4), 553-570, 2001.

1122 Kollat, J. B. and Reed, P. M.: Comparing state-of-the-art evolutionary multi-objective  
1123 algorithms for long-term groundwater monitoring design, *Adv. Water Resour.*, 29, 792-807,  
1124 2006.

1125 Li, H. Y., Sivapalan, M. and Tian, F. Q.: Comparative diagnostic analysis of runoff generation  
1126 processes in Oklahoma DMIP2 basins: The Blue River and the Illinois River, *J. Hydrol.*, 418,  
1127 90-109, 2012.

1128 Li, X. G. and Williams M. W.: Snowmelt runoff modelling in an arid mountain watershed,  
1129 Tarim Basin, China, *Hydrol. Process.*, 22 (19SI), 3931-3940, 2008.

1130 Liu, D. F., Tian, F. Q., Hu, H. C. and Hu, H. P.: The role of run-on for overland flow and the  
1131 characteristics of runoff generation in the Loess Plateau, China, *Hydrolog. Sci. J.*, 57, 1107-  
1132 1117, 2012.

1133 Liu, S. Y., Xie, Z. C., Wang, N. L. and Ye, B. S.: Mass balance sensitivity to climate change:  
1134 a case study of glacier no. 1 at Urumqi riverhead, Tianshan mountains, China, *Chin. Geogr.*  
1135 *Sci.*, 9, 134-140, 1999.

1136 Liu, T., Willems, P., Feng, X. W., Li, Q., Huang, Y., Bao, A. M., Chen, X., Veroustraete, F.  
1137 and Dong, Q. H.: On the usefulness of remote sensing input data for spatially distributed  
1138 hydrological modelling: case of the Tarim River basin in China, *Hydrol. Process.*, 26 (3),

1139 335-344, 2012.

1140 Lopez-Burgos, V., Gupta, H. V. and Clark, M.: A probability of snow approach to removing  
1141 cloud cover from MODIS Snow Cover Area products, *Hydrol. Earth Syst. Sci. Discuss*, 9,  
1142 13693-13728, 2012.

1143 Luo, Y., Arnold, J., Liu, S., Wang, X. and Chen, X.: Inclusion of glacier processes for  
1144 distributed hydrological modeling at basin scale with application to a watershed in Tianshan  
1145 Mountains, northwest China, *J. Hydrol.*, 477, 72-85, 2013.

1146 Martinec, J., Oeschger, H., Schotterer, U. and Siegenthaler, U.: Snowmelt and groundwater  
1147 storage in alpine basin, In *Hydrological Aspects of Alpine and High Mountain Areas*,  
1148 Wallingford, United Kingdom: IAHS Press, 169–175, 1982.

1149 McCuen, R. H.: *Hydrologic analysis and design*, Prentice Hall, New Jersey pp.355-360, 1989.

1150 Mendoza, G. F., Steenhuis, T. S., Walter, M. T. and Parlange, J. Y.: Estimating basin-wide  
1151 hydraulic parameters of a semi-arid mountainous watershed by recession-flow analysis, *J.*  
1152 *Hydrol.*,279,57-69,2003.

1153 Mou, L., Tian, F., Hu, H. and Sivapalan, M.: Extension of the Representative Elementary  
1154 Watershed approach for cold regions: constitutive relationships and an application, *Hydrol.*  
1155 *Earth Syst. Sci.*, 12, 565-585, 2008.

1156 Mu, Z. X. and Jiang, H. F.: Establishment of snowmelt type Xin'anjiang watershed model based  
1157 on digital elevation model, *Journal of Xinjiang Agricultural University*, 5 (32), 75-80, 2009  
1158 (in Chinese).

1159 Nash, J. E. and Sutcliffe, J. V.: River flow forecasting through conceptual models part I — A  
1160 discussion of principles, *J. Hydrol.*, 10, 282-290, 1970.

1161 Nathan, R. J., McMahon, T. A.: Evaluation of automated techniques for base flow and recession  
1162 analyses, *Water Resour. Res.*, 26, 1465-1473, 1990.

1163 Nejadhashemi, A. P., Shirmohammadi, A., Sheridan, J. M., Montas, H. J. and Mankin, K. R.:  
1164 Case Study: Evaluation of Streamflow Partitioning Methods, *J. Irrig. Drain. Eng.*, 135, 791-  
1165 801, 2009.

1166 Pellicciotti, F., Brock, B., Strasser, U., Burlando, P., Funk, M. and Corripio, J.: An enhanced  
1167 temperature-index glacier melt model including the shortwave radiation balance:  
1168 development and testing for Haut Glacier d'Arolla, Switzerland, *Journal of Glaciology*, 51  
1169 (175), 573-587, 2005.

1170 Pinder, G. F. and Jones, J. F.: Determination of the ground-water component of peak  
1171 Determination of the ground-water component of peak discharge from the chemistry of total  
1172 runoff, *Water Resour. Res.*, 5, 438-445, 1969.

1173 Rango, A. and Martinec, J.: Application of a Snowmelt-runoff Model Using Landsat Data, *Nord.*  
1174 *Hydrol.*, 10, 225-238, 1979.

1175 Richter, B. D., Baumgartner, J. V., Powell, J. and Braun, D. P.: A method for assessing  
1176 hydrologic alteration within ecosystems, *Conservation Biology*, 10, 1163-1174, 1996.

1177 Schaefli, B. and Gupta, H. V.: Do Nash values have value, *Hydro. Process.*, 21 (15), 2075-2080,  
1178 2007.

1179 Schaefli, B., Hingray, B., Niggli, M. and Musy, A.: A conceptual glacio-hydrological model  
1180 for high mountainous catchments, *Hydrol. Earth Syst. Sci.*,9 (1-2), 95-109, 2005.

1181 Schaefli, B. and Huss, M.: Integrating point glacier mass balance observations into hydrologic  
1182 model identification, *Hydrol. Earth Syst. Sci.*,15,1227-1241,2011.

1183 Shamir, E., Imam, B., Gupta, H. V. and Sorooshian, S.: Application of temporal streamflow  
1184 descriptors in hydrologic model parameter estimation, *Water Resour. Res.*, 41, W06021,  
1185 doi:10.1029/2004WR003409, 2005a.

1186 Shamir, E., Imam, B., Morin, E., Gupta, H. V. and Sorooshian, S.: The role of hydrograph  
1187 indices in parameter estimation of rainfall-runoff models, *Hydrol. Process.*, 19, 2187-2207,  
1188 2005b.

1189 Shen, Y., Liu, S., Ding, Y. and Wang, S.: Glacier Mass Balance Change in Tailanhe River  
1190 Watersheds on the South Slope of the Tianshan Mountains and its impact on water resources,  
1191 *Journal of Glaciology and Geocryology*, 25, 124-129, 2003(in Chinese).

1192 Shi, Y.: *Concise Glacier Inventory of China*, Shanghai Popular Science Press., Shanghai, China,  
1193 2008(in Chinese).

1194 Singh, P., Kumar, N. and Arora, M.: Degree-day factors for snow and ice for Dokriani Glacier,  
1195 Garhwal Himalayas, *J. Hydrol*, 235, 1-11, 2000.

1196 Sivapalan, M., Bloschl, G., Zhang, L. and Vertessy, R.: Downward approach to hydrological  
1197 prediction, *Hydrol. Process.*, 17, 2101-2111, 2003.

1198 Sorooshian, S. and Gupta, V. K.: Automatic calibration of conceptual rainfall-runoff models-  
1199 the question of parameter observability and uniqueness, *Water Resour. Res.*, 19, 260-268,  
1200 1983.

1201 Spear, R. C. and Hornberger, G. M.: Eutrophication in peel inlet—II. Identification of critical  
1202 uncertainties via generalized sensitivity analysis, *Water Research*, 14, 43-49, 1980.

1203 Stahl, K., Moore, R. D., Shea, J. M., Hutchinson, D. and Cannon, A. J.: Coupled modelling of  
1204 glacier and streamflow response to future climate scenarios, *Water Resour. Res.*, 44, 2008.

1205 Sun, M., Yao, X., Li, Z. and Li, J.: Estimation of Tailan River Discharge in the Tianshan  
1206 Mountains in the 21st Century, *Advances on Climate Change Research*, 8, 342-349, 2012(in  
1207 Chinese).

1208 Swamy, A. N. and Brivio, P. A.: Modelling runoff using optical satellite remote sensing data  
1209 in a high mountainous alpine catchment of Italy, *Hydrol. Process.*, 11 (11), 1475-1491, 1997.

1210 Tabony, R. C.: The variation of surface temperature with altitude, *Meteorological Magazine*,  
1211 114, 37-48, 1985.

1212 Tahir, A. A., Chevallier, P., Arnaud, Y., Neppel, L. and Ahmad, B.: Modeling snowmelt-runoff  
1213 under climate scenarios in the Hunza River basin, Karakoram Range, Northern Pakistan, *J.*  
1214 *Hydrol*, 409, 104-117, 2011.

1215 Tian, F. Q., Hu, H. P. and Lei, Z. D.: Thermodynamic watershed hydrological model:  
1216 Constitutive relationship, *Science in China, Ser. E-Technological Sciences*, 51, 1353-1369,  
1217 2008.

1218 Tian, F., Hu, H., Lei, Z. and Sivapalan, M.: Extension of the Representative Elementary  
1219 Watershed approach for cold regions, *Hydrol. Earth Syst. Sci.*, 10, 619-644, 2006.

1220 Tian, F. Q., Li, H. Y. and Sivapalan, M.: Model diagnostic analysis of seasonal switching of  
1221 runoff generation mechanisms in the Blue River basin, Oklahoma, *J. Hydrol*, 418, 136-149,  
1222 2012.

1223 Van Griensven, A. and Bauwens, W.: Multiobjective autocalibration for semidistributed water  
1224 quality models, *Water Resour. Res.*, 39, 1348, 2003.

1225 Van Straten, G. T. and Keesman, K. J.: Uncertainty propagation and speculation in projective  
1226 forecasts of environmental change: A lake-eutrophication example, *J. Forecast.*, 10, 163-190,

1227 1991.

1228 Vivoni, E. R., Entekhabi, D., Bras, R. L. and Ivanov, V. Y.: Controls on runoff generation and  
1229 scale-dependence in a distributed hydrologic model, *Hydrol. Earth Syst. Sci.*, 11, 1683-1701,  
1230 2007.

1231 Vrugt, J. A., Gupta, H. V., Bastidas, L. A., Bouten, W. and Sorooshian, S.: Effective and  
1232 efficient algorithm for multiobjective optimization of hydrologic models, *Water Resour. Res.*,  
1233 39, 1214, 2003a.

1234 Vrugt, J. A., Gupta, H. V., Bouten, W. and Sorooshian, S.: A Shuffled Complex Evolution  
1235 Metropolis Algorithm for Optimization and Uncertainty Assessment of Hydrological Model  
1236 Parameters, *Water Resour. Res.*, 39, 1201, doi:10.1029/2002WR001642, 8., 2003b.

1237 Wang, X. W., Xie, H. J., Liang, T. G. and Huang, X. D.: Comparison and validation of MODIS  
1238 standard and new combination of Terra and Aqua snow cover products in northern Xinjiang,  
1239 China, *Hydrol. Process.*,23, 419-429, 2009.

1240 Westerberg, I. K., Guerrero, J. L., Younger, P. M., Beven, K. J., Seibert, J., Halldin, S., Freer,  
1241 J. E. and Xu, C. Y.: Calibration of hydrological models using flow-duration curves, *Hydrol.*  
1242 *Earth Syst. Sci.*,15 (7), 2205-2227, 2011.

1243 Wu, J., L. L.:A rain-on-snow mixed flood forecast model and its application, *Engineering*  
1244 *Journal of Wuhan University*,40,20-23,2007(in Chinese).

1245 Xie, C., Ding, Y., Liu, S. and Han, H.: Analysis on the Glacial Hydrological Features of the  
1246 Glaciers on the South Slope of Mt. Tuomuer and the Effects on Runoff, *Arid Land*  
1247 *Geography*, 27, 570-575, 2004(in Chinese).

1248 Yadav, M., Wagener, T. and Gupta, H.: Regionalization of constraints on expected watershed  
1249 response behavior for improved predictions in ungauged basins, *Adv. Water Resour*, 30,  
1250 1756-1774, 2007.

1251 Yang, D. Q., Zhao, Y. Y., Armstrong, R., Robinson, D. and Brodzik, M. J.: Streamflow  
1252 response to seasonal snow cover mass changes over large Siberian watersheds, *J. Geophys.*  
1253 *Res.*, 112, F02S22F2, 2007.

1254 Yang, X. S., Jiang, H. F., Huang, C. R. Zheng, Z., and Yong, G.: An applied study on the  
1255 snowmelt type of Xin'anjiang watershed model at the Kaidu river basin, *Journal of Xinjiang*  
1256 *Agricultural University*,4, 82-90, 1987 (in Chinese).

1257 Yilmaz, K. K., Gupta, H. V. and Wagener, T.: A process-based diagnostic approach to model  
1258 evaluation: Application to the NWS distributed hydrologic model, *Water Resour. Res.*,  
1259 44,W09417, doi:10.1029/2007WR006716, 2008.

1260 Zhang, Z. X., Wagener, T., Reed, P. and Bhushan, R.: Reducing uncertainty in predictions in  
1261 ungauged basins by combining hydrologic indices regionalization and multiobjective  
1262 optimization, *Water Resour. Res.*, 44 (W00B04), doi:10.1029/2008WR006833, 2008.

1263 Zhao, R. J.: The Xin'anjiang model applied in China, *J. Hydrol*,135,371-381,1992.

1264

Table1. Estimated monthly temperature lapse rate in the TRB

Month	Temperature lapse rate (°C/day/100 m)
January	-0.38
February	-0.38
March	-0.66
April	-0.76
May	-0.80
June	-0.78
July	-0.82
August	-0.86
September	-0.66
October	-0.60
November	-0.54
December	-0.30
Annual	-0.62

1265

1266

Table 2. Estimated week-precipitation lapse rate in storm rain months

Month	Precipitation lapse rate (mm/week/ 100 m)
May	1.63
June	1.69
July	3.14
August	2.40
September	2.28

1267

1268  
1269

Table 3. Grouped parameters in the THREW model. Parameters subjected to calibration are highlighted in red.

Category	Symbol	Unit	Description	Value
Subsurface	$K_s^u$	m s <sup>-1</sup>	Saturated hydraulic conductivity for u-zone	1.25E-05
	$K_s^s$	m s <sup>-1</sup>	Saturated hydraulic conductivity for s-zone	1.25E-05
	$K_A$	-	Coefficient used to calculate subsurface flow	Calibrated
	$K_D$	-	Coefficient used to calculate subsurface flow	Calibrated
Routing	$n^t$	-	Manning roughness coefficient for hillslope, obtained from the literature according to land use and vegetation type	1.50E-01
	$n^r$	-	Similar to $n^t$ , roughness coefficient for channel	3.00E-01
Infiltration	$\alpha^{EFL}$	-	Spatial heterogeneous coefficient for exfiltration capacity	1.00E+00
	$\alpha^{IFL}$	-	Spatial heterogeneous coefficient for infiltration capacity	1.50E+00
Interception	$F \max^b$	m	Ground surface depression storage capacity	0.00E+00
	$\alpha^{vb}$	m	Maximum rainfall depth a single leaf can intercept and hold	1.00E-05
Rainfall runoff	$B$	-	Shape coefficient to calculate the saturation excess runoff area from the Xin'anjiang model	Calibrated
	$W_M$	cm	Spatial averaged tension water storage capacity in the Xin'anjiang model	Calibrated
Melt	$D_g$	mm °C <sup>-1</sup> day <sup>-1</sup>	Glacier melt degree day factor	Calibrated
	$D_s$	mm °C <sup>-1</sup> day <sup>-1</sup>	Snowmelt degree day factor	Calibrated

1270

1271

Table 4. Calibrated parameters by the stepwise and automatic methods

Parameter	Stepwise Calibrated	Automatic Calibrated
$K_A$	1.1	5.6
$K_D$	0.002	99.1
$D_s(\text{mm } ^\circ\text{C}^{-1} \text{ day}^{-1})$	2.5	2.03
$D_g(\text{mm } ^\circ\text{C}^{-1} \text{ day}^{-1})$	7.2	7.52
$W_M(\text{cm})$	10.5	11.9
$B$	0.80	0.62

1272



Table 5. Evaluation merits for the stepwise and automatic calibration methods

Merits	Calibration period	Calibration period	Calibration period	Evaluation period	Evaluation period
	Automatic method	Stepwise method	Benchmark model	Stepwise method	Benchmark model
$RMSEln(Q_{SB}, m^3/s)$	0.352	0.302	-	0.213	-
$RMSE(Q_{SB}+Q_{SM}, m^3/s)$	2.807	1.811	-	1.762	-
$RMSE(Q_{SB}+Q_{SM}+Q_{GM}, m^3/s)$	6.079	4.784	-	4.558	-
$RMSE(Q_{SB}+Q_{SM}+Q_{GM}+Q_R, m^3/s)$	13.245	12.650	-	16.727	-
$NSE$	0.867	0.881	0.815	0.752	0.577
$NSEln$	0.841	0.929	0.923	0.894	0.844
$RMSE (m^3/s)$	8.990	8.459	10.534	11.021	14.381
$BE$	0.271	0.355	-	0.413	-

1275 Table 6. Sensitive analysis of the calibrated parameters on lowest elevation band for glacier  
 1276 area (LEG) and storm rain period (SRP). *NSE* is the Nash Sutcliffe Efficiency value for the  
 1277 calibration period.

	LEG(a.s.l. m)	$D_s(\text{mm/d/}^\circ\text{C})$	$D_g(\text{mm/d/}^\circ\text{C})$	$W_M(\text{cm})$	$B$	$K_A$	$K_D$	$NSE$
	3450	2.2	8.0	10.1	0.70	0.7	0.002	0.870
	3150	2.5	7.9	10.1	0.75	0.7	0.002	0.871
SRP:	2950	2.5	7.2	10.5	0.80	1.1	0.002	0.881
May. To Sep.	2750	3.0	6.8	10.2	0.75	1.0	0.002	0.880
	2450	2.8	5.8	10.0	0.78	0.8	0.002	0.876
	SRP	$D_s(\text{mm/d/}^\circ\text{C})$	$D_g(\text{mm/d/}^\circ\text{C})$	$W_M(\text{cm})$	$B$	$K_A$	$K_D$	$NSE$
	Jun. to Aug.	2.9	7.5	8.2	0.75	0.9	0.002	0.871
	May. to Oct.	2.8	6.9	9.4	0.76	0.8	0.002	0.882
LEG=2950m	May. to Sep.	2.5	7.2	10.5	0.80	1.1	0.002	0.881
	Apr. to Sep.	2.2	7.1	8.3	0.75	0.9	0.002	0.878
	Apr. to Oct.	2.6	6.9	9.4	0.77	1.1	0.002	0.881

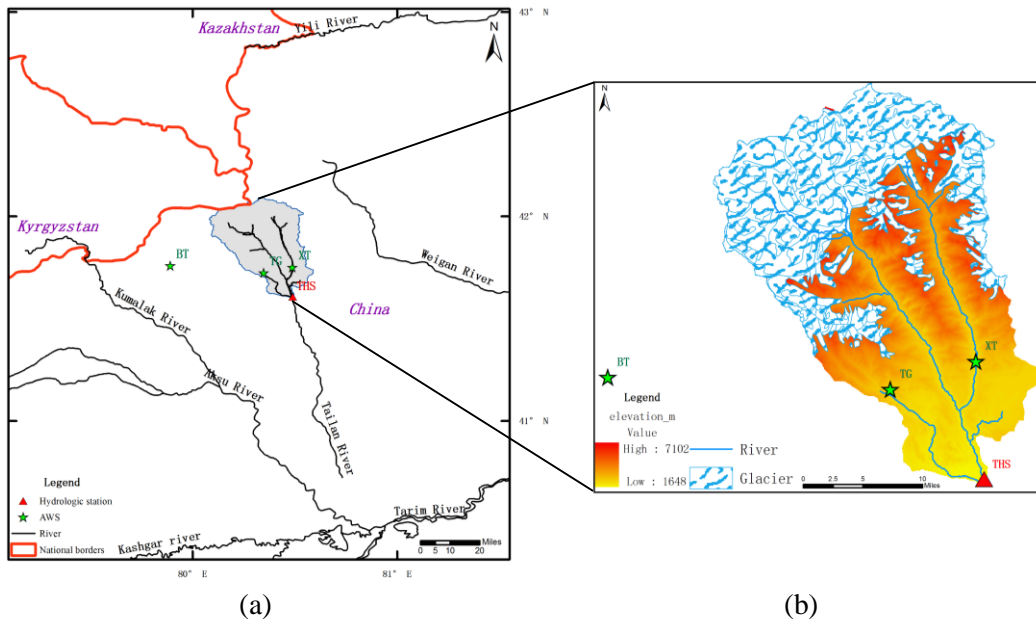
1278

1279  
1280

Table 7.  $R_{MS}$  (%) for parameter sensitivity ( $R_{MS}$  values indicating the most sensitive parameters are labeled in bold and red)

Merits	Subsurface				Routing	Infiltration	Interception	Rainfall Runoff		Melt	
	$K_s^u$	$K_s^s$	$K_A$	$K_D$	$n^t$	$\alpha^{IFL}$	$F \max^b$	$W_M$	$B$	$D_s$	$D_g$
<i>RMSE</i> <sub>ln</sub> ( $Q_{SB}$ )	9.70	11.14	<b>38.44</b>	<b>44.39</b>	15.70	0.12	0.08	1.07	18.51	7.53	2.88
<i>RMSE</i> ( $Q_{SB}+Q_{SM}$ )	0.32	0.40	11.91	0.06	9.35	0.47	0.14	8.27	25.14	<b>51.22</b>	0.69
<i>RMSE</i> ( $Q_{SB}+Q_{SM}+Q_{GM}$ )	0.22	0.21	0.62	0.64	10.00	0.17	0.25	7.92	0.29	26.28	<b>40.79</b>
<i>RMSE</i> ( $Q_{SB}+Q_{SM}+Q_{GM}+Q_R$ )	0.17	0.85	0.57	0.97	1.84	0.08	0.06	<b>19.35</b>	<b>22.48</b>	10.78	11.57

1281

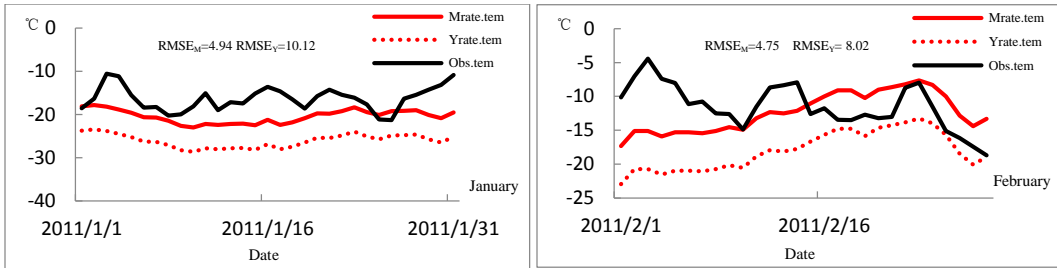


1282  
 1283  
 1284  
 1285  
 1286  
 1287  
 1288  
 1289  
 1290

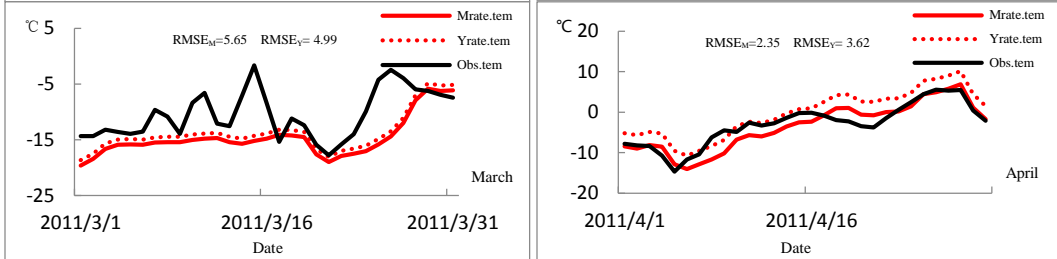
(a) (b)

Figure 1. Location of the Tailan River basin in Xinjiang Uygur Autonomous Region, China. Two automatic weather stations (TG at 2381 m a.s.l. and XT at 2116 m a.s.l.) were set up in upstream mountain area in July, 2011. Additionally, the BT weather station (3950 m a.s.l.) located in the adjacent Kumalak River basin was used to validate the estimated temperature lapse rates. The Tailan Hydrologic Station (THS) has gauged streamflow data at the catchment outlet since 1957(a). Glacier occupies approximately 33% of the total basin area (b).

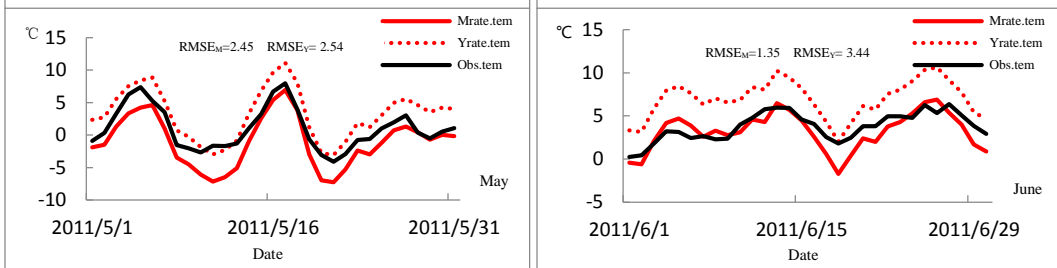
1291



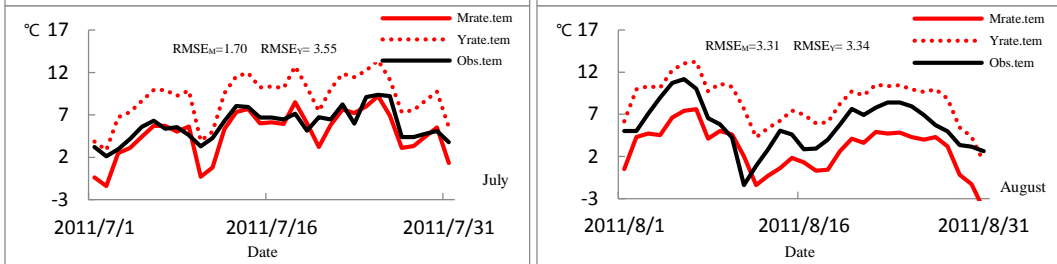
1292



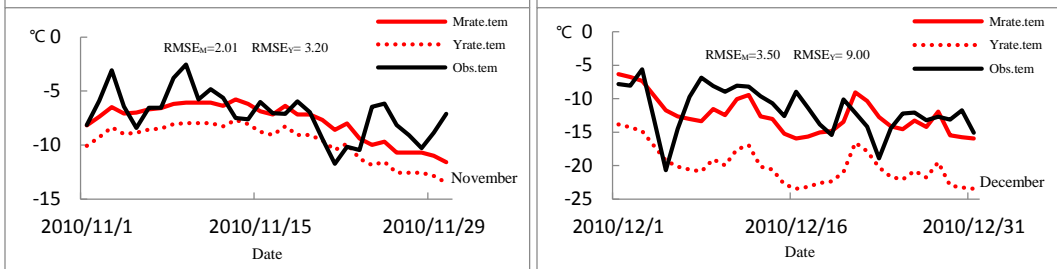
1293



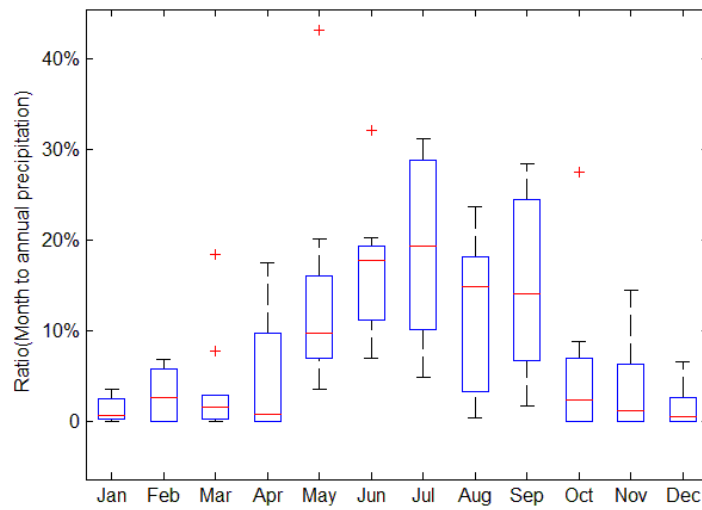
1294



1295

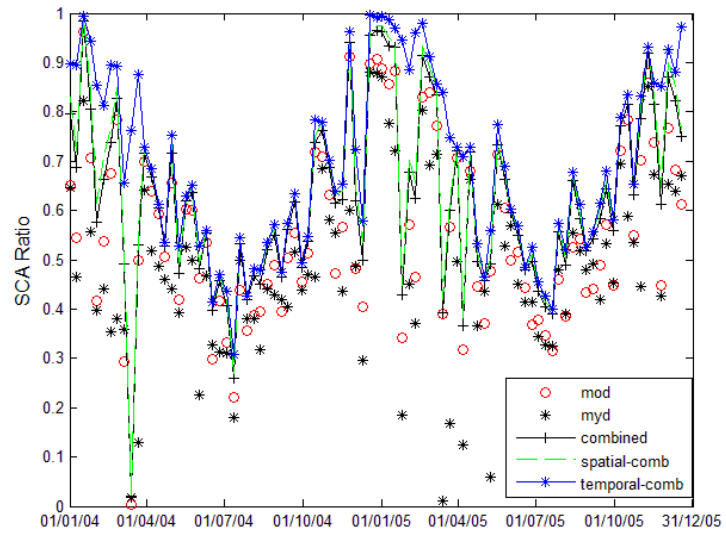


1296 Figure 2. Evaluation of the estimated temperature lapse rate at the BT station. The black solid  
 1297 line is the observed temperature series at BT (Obs.tem); the red solid line is the estimated  
 1298 temperature by monthly lapse rate (Mrate.tem).The red dotted line indicates the estimated  
 1299 temperature based on annual constant rate (Yrate.tem). The goodness of fit between the  
 1300 observed and estimated temperature is measured by  $RMSE_M$  for monthly lapse rate and  
 1301  $RMSE_Y$  for annual constant rate, respectively. The temperature series in September and  
 1302 October are absent at BT.



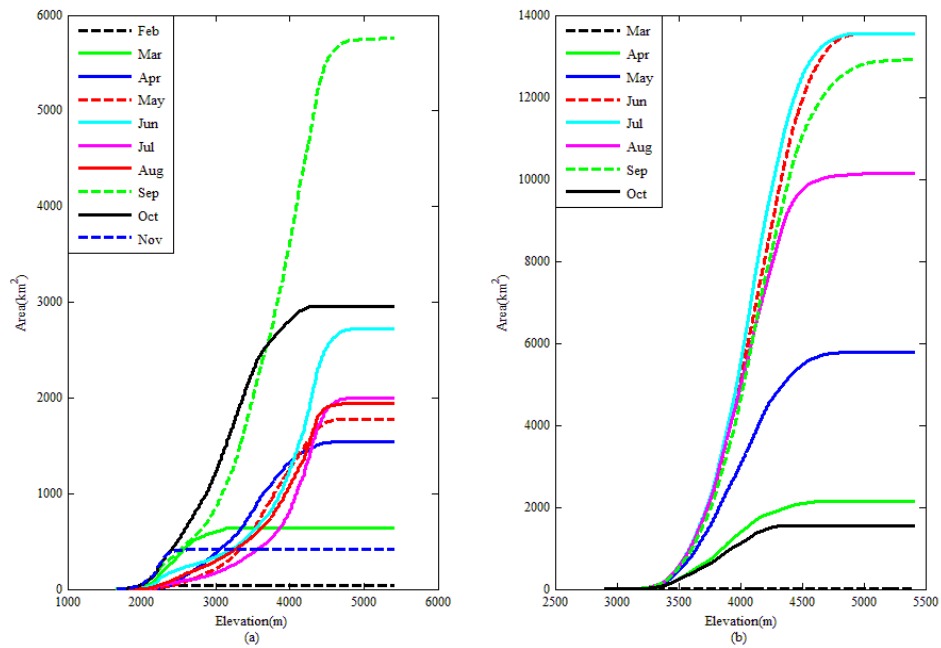
1303

1304 Figure 3. Proportion of monthly precipitation to annual amount (2003~2012). The red line in  
 1305 each box represents the median value for each month from 2003 to 2012. Red crosses indicate  
 1306 abnormal values that exceed 1.5 times the inter quartile range.



1307  
 1308  
 1309  
 1310  
 1311

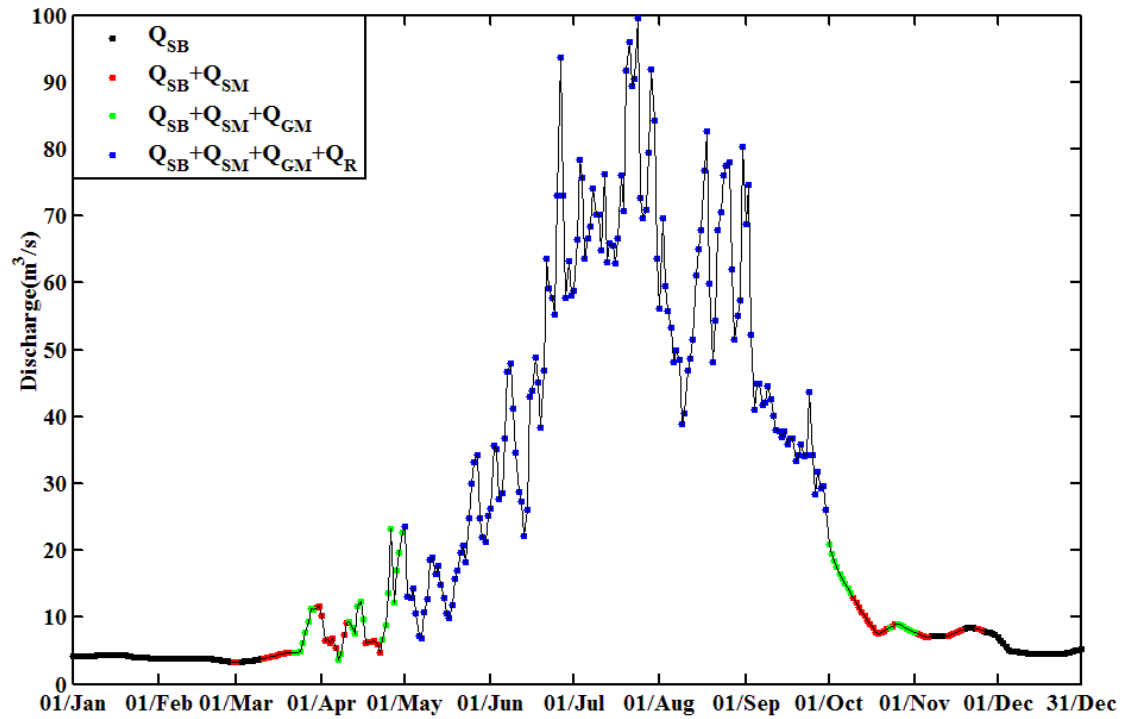
Figure 4. Filtered MODIS eight-day snow-cover products (2004-2005). The term ‘mod’ is the snow cover area from MOD10A2 products, ‘myd’ is MYD10A2 products, ‘combined’ is the combined result from step1, ‘spatial-comb’ from step2 and ‘temporal-comb’ from step3. See Sect. 2.2.3 for details.



1312  
 1313  
 1314  
 1315  
 1316  
 1317

Figure 5. Altitudinal Cumulative Melt Curve. (a) Cumulative monthly snowmelt area distribution by elevation (2003~2012). (b) Cumulative monthly glacier melt area distribution by elevation (2003~2012). The snowmelt areas in December and January and the glacier melt areas in November, December, January and February are zero and are not shown in this figure.





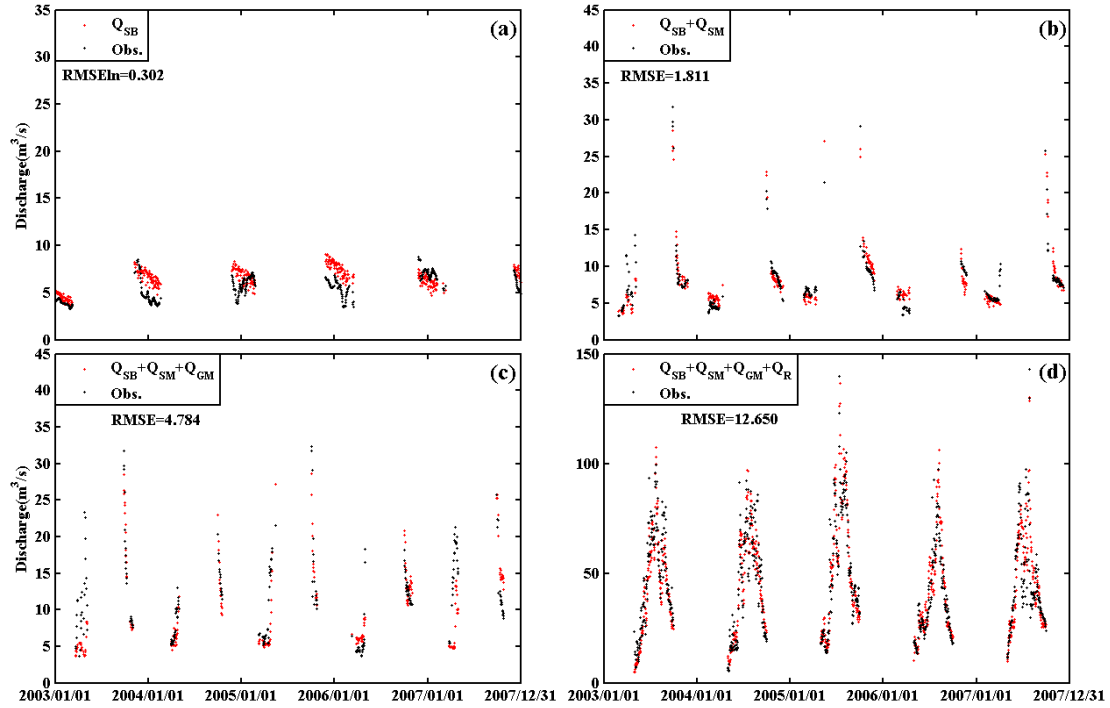
1318

1319

1320

1321

Figure 6. Hydrograph partition in 2003.  $Q_{SB}$  stands for subsurface baseflow generated by groundwater,  $Q_{SM}$  and  $Q_{GM}$  for snow meltwater and glacier meltwater respectively, and  $Q_R$  for rainwater directly runoff.



1322

1323

1324

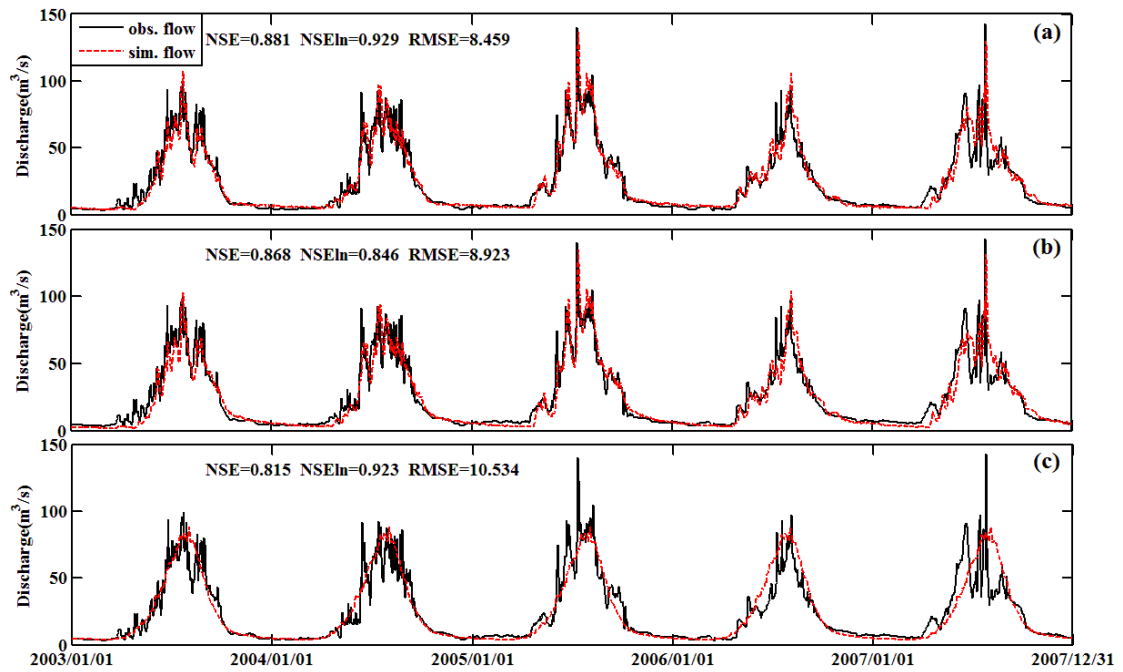
1325

1326

1327

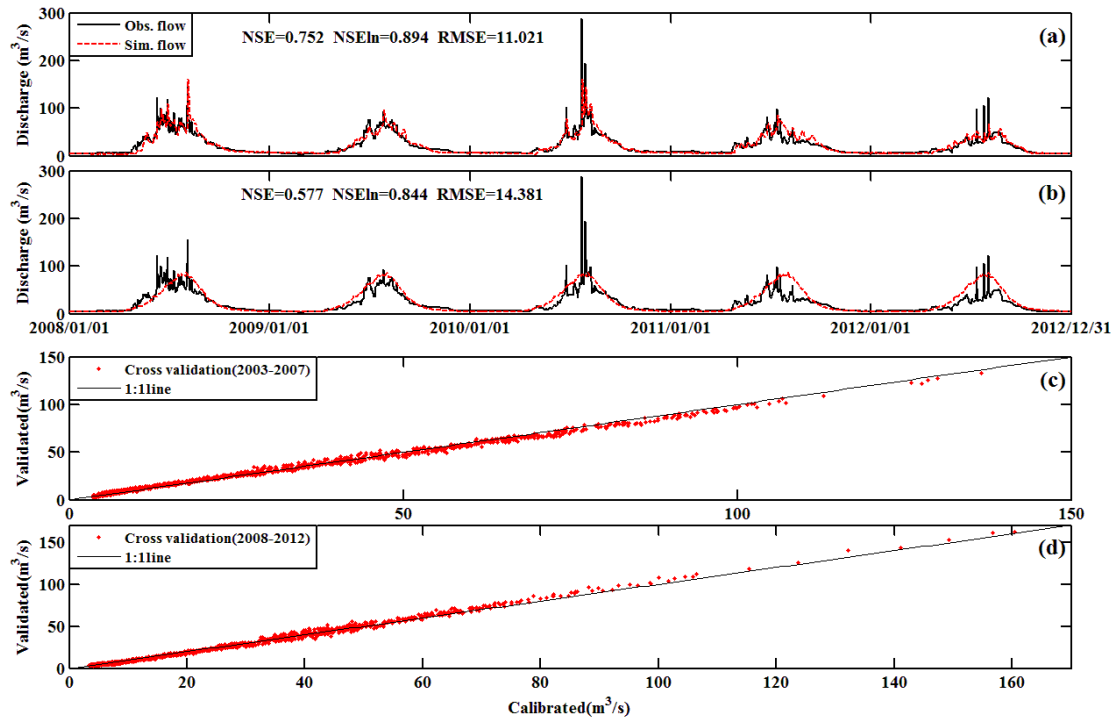
1328

Figure 7. Stepwise calibration of grouped parameters upon partitioning curves. (a) Partitioning curves after calibrating  $K_A$  and  $K_D$  upon  $Q_{SB}$ . (b) Partitioning curves after calibrating  $D_s$  upon  $Q_{SB}+Q_{SM}$ . (c) Partitioning curves after calibrating  $D_g$  upon  $Q_{SB}+Q_{SM}+Q_{GM}$ . (d) Partitioning curves after calibrating  $W_M$  and  $B$  upon  $Q_{SB}+Q_{SM}+Q_{GM}+Q_R$ . The goodness of fit between observed and simulated discharge is measured by  $RMSEln$  (for  $Q_{SB}$  part) or  $RMSE$  (for other parts).



1329  
 1330  
 1331  
 1332

Figure 8. Simulation of daily streamflow by different methods from 2003 to 2007. (a) by the proposed stepwise method, (b) by the automatic calibration method, and (c) by the benchmark model. The performance of the simulations is measured in *NSE*, *NSEln* and *RMSE*.



1333

1334

1335

1336

1337

1338

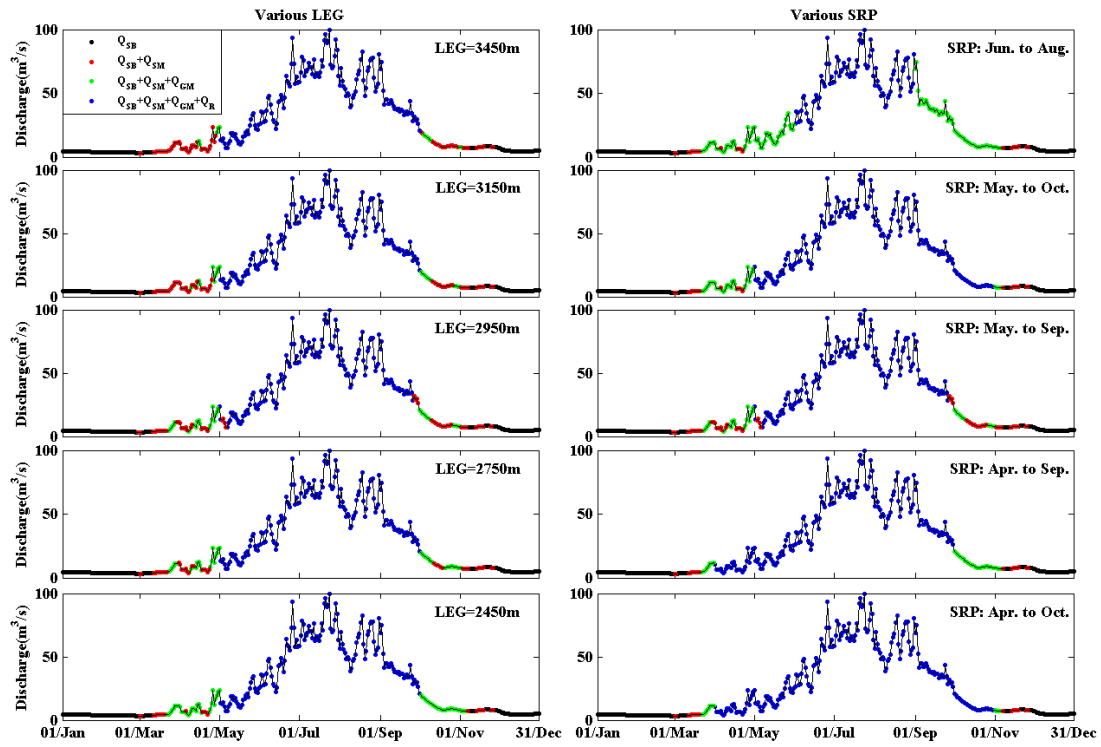
1339

1340

1341

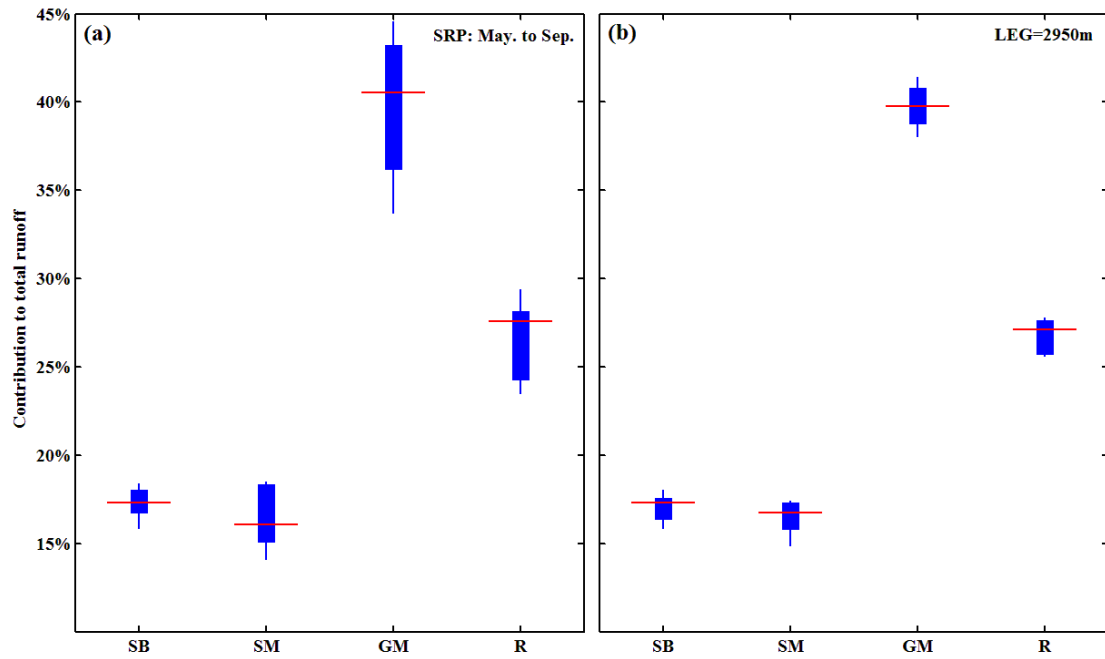
1342

Figure 9. Evaluation of the stepwise calibration method. (a) discharge simulation in evaluation period 2008 to 2012 using the stepwise calibrated parameters in calibration period 2003 to 2007. (b) discharge simulation in evaluation period 2008 to 2012 by the benchmark model. (c) Cross validation simulation of daily discharge in 2003-2007. x-coordinate presents the simulated daily discharges by parameters calibrated in period 2003-2007. y-coordinate presents the simulated daily discharges by parameters calibrated in period 2008-2012. (d) Cross validation simulation of daily discharge in 2008-2012. x-coordinate presents the simulated daily discharges by parameters calibrated in period 2008-2012. y-coordinate presents the simulated daily discharges by parameters calibrated in period 2003-2007.



1343  
 1344  
 1345  
 1346  
 1347

Figure 10. Sensitivity analysis for hydrograph partition. The first column is the hydrograph partition pattern using different lowest elevation band of the glacier area (LEG). The second column is the hydrograph partition pattern using different storm rain period (SRP).



1348

1349

1350

1351

1352

1353

1354

1355

1356

Figure 11. Sensitivity analysis on the contributions of different runoff sources to total runoff. (a) is the contribution pattern under different lowest elevation band of glacier area (LEG), where the storm rain period (SRP) is fixed as May to September. (b) is the contribution pattern under different SRPs, where the LEG is fixed as 2950m. The red line stands for the mean contribution for each runoff source, and the top/bottom end of each plot presents the highest/lowest contribution ratio. SB is groundwater baseflow, SM is snowmelt, GM is glacier melt and R is rainwater directly runoff.